ORNL/TM-2015/171

FY15 Status Report: CIRFT Testing of Used Nuclear Fuel Rods from the Limerick Generating Station Boiling Water Reactor

Fuel Cycle Research & Development

Prepared for
US Department of Energy
Used Fuel Disposition Campaign

J.-A. Wang, H. Wang, and H. Jiang
B. B. Bevard
Oak Ridge National Laboratory

April 30, 2015
FCRD-UFD-2015-000635

ORNL/TM-2015/171

Materials Science and Technology Division

FY15 Status Report: CIRFT Testing of Used Nuclear Fuel Rods from the Limerick Generating Station Boiling Water Reactor

Jy-An John Wang, Hong Wang, and Hao Jiang

Program Manager
Bruce Bevard

Date Published: April 30, 2015

Prepared by
OAK RIDGE NATIONAL LABORATORY
Oak Ridge, Tennessee 37831-6283
managed by
UT-BATTELLE, LLC
for the
US DEPARTMENT OF ENERGY
under contract DE-AC05-00OR22725

This page intentionally left blank.

TABLE OF CONTENTS

This page intentionally left blank.

LIST OF FIGURES

This page intentionally left blank.

LIST OF TABLES

This page intentionally left blank.

SUMMARY

The objective of this project is to perform a systematic study of spent nuclear fuel (SNF, also known as "used nuclear fuel" [UNF]) integrity under simulated transportation environments using the Cyclic Integrated Reversible-Bending Fatigue Tester (CIRFT) hot-cell testing technology developed at Oak Ridge National Laboratory (ORNL) in August 2013. Under Nuclear Regulatory Commission (NRC) sponsorship, ORNL completed four benchmark tests, four static tests, and twelve dynamic or cycle tests on H. B. Robinson (HBR) high burn-up (HBU) fuel. The clad of the HBR fuels was made of Zircaloy-4. Testing was continued in fiscal year (FY) 2014 using Department of Energy (DOE) funds. Additional CIRFT testing was conducted on three HBR rods; two specimens failed, and one specimen was tested to over 2.23×10^7 cycles without failing. The data analysis on all the HBR SNF rods demonstrated that it is necessary to characterize the fatigue life of the SNF rods in terms of (1) the curvature amplitude and (2) the maximum absolute of curvature extremes. The maximum extremes are significant because they signify the maximum tensile stress for the outer fiber of the bending rod. CIRFT testing has also addressed a large variation in hydrogen content on the HBR rods. While the load amplitude is the dominant factor that controls the fatigue life of bending rods, the hydrogen content also has an important effect on the lifetime attained at each load range tested.

In FY 15, eleven SNF rod segments from the Limerick BWR were tested using the ORNL CIRFT equipment; one test under static conditions and ten tests under dynamic loading conditions.

Under static unidirectional loading, a moment of 85 N·m was obtained at a maximum curvature of 4.0 m^{-1}. The specimen did not show any sign of failure during three repeated loading cycles to a similar maximum curvature.

Ten cyclic tests were conducted with amplitudes varying from 15.2 to 7.1 N·m. Failure was observed in nine of the tested rod specimens. The cycles-to-failure ranged from 1.22×10^5 to 4.70×10^6, and the amplitudes varied from 15.2 to 7.6 N·m. The measurements at the interrupts indicated a range of flexural rigidity from 30 to 50 $N \cdot m^2$. Online monitoring revealed that the flexural rigidity was slightly lower due to the higher loading, from 25 to 42 $N \cdot m^2$. Generally, no substantial change of rigidity was observed based on the online monitoring during the cyclic fatigue testing process. Overall, the decreasing trend of sample lifetime with increasing amplitude is well defined.

This page intentionally left blank.

1. INTRODUCTION

The objective of this activity is to collect experimental data on spent nuclear fuel (SNF) from the Limerick Generating Station boiling water reactor (BWR) under simulated transportation environments using the Cyclic Integrated Reversible-Bending Fatigue Tester (CIRFT), the enabling hot-cell testing technology developed recently at Oak Ridge National Laboratory (ORNL). [1,2,3,4,5] This data will be utilized to support ongoing spent fuel modeling activities.

The testing on SNF rods from pressurized water reactors (PWRs)—H. B. Robinson (Zircaloy 4 cladding), North Anna (Zircaloy 4 cladding), and Catawba (M5™ cladding)[6,7,8]—demonstrated that the cyclic fatigue lifetime of SNF rods generally depends on the amplitude of applied moment when a 5-Hz waveform is used. It was also demonstrated that the lifetime of SNF is related to the degree of damage in cladding and fuel pellets arising from irradiation from long-term service inside a reactor, as well as the loading amplitude of applied moment, due to different fatigue damage mechanism triggered by the intensity of pellet-clad mechanical interaction. The current activity extends the vibration data collected to include Zircaloy-2 data from a BWR environment. An S-N trend similar to that of PWR data was also observed in the BWR data. Furthermore, the accumulated damage from the combination of low amplitude CIRFT cyclic bending plus transient shocks (high amplitude bending load) indicates an accelerated aging effect compared to that of low amplitude cyclic bend loading alone.

2. CUTTING PLAN FOR LIMERICK RODS

Twenty CIRFT testing segments were prepared as six-inch segments from four parent Limerick rods. The cutting plan is shown in Fig. 1, and the corresponding segment identification numbers (IDs) are given in Table 1. The outer diameters (ODs) were measured to be 0.44971 inches and 0.44663 inches for two segments, as shown in

Table 2.

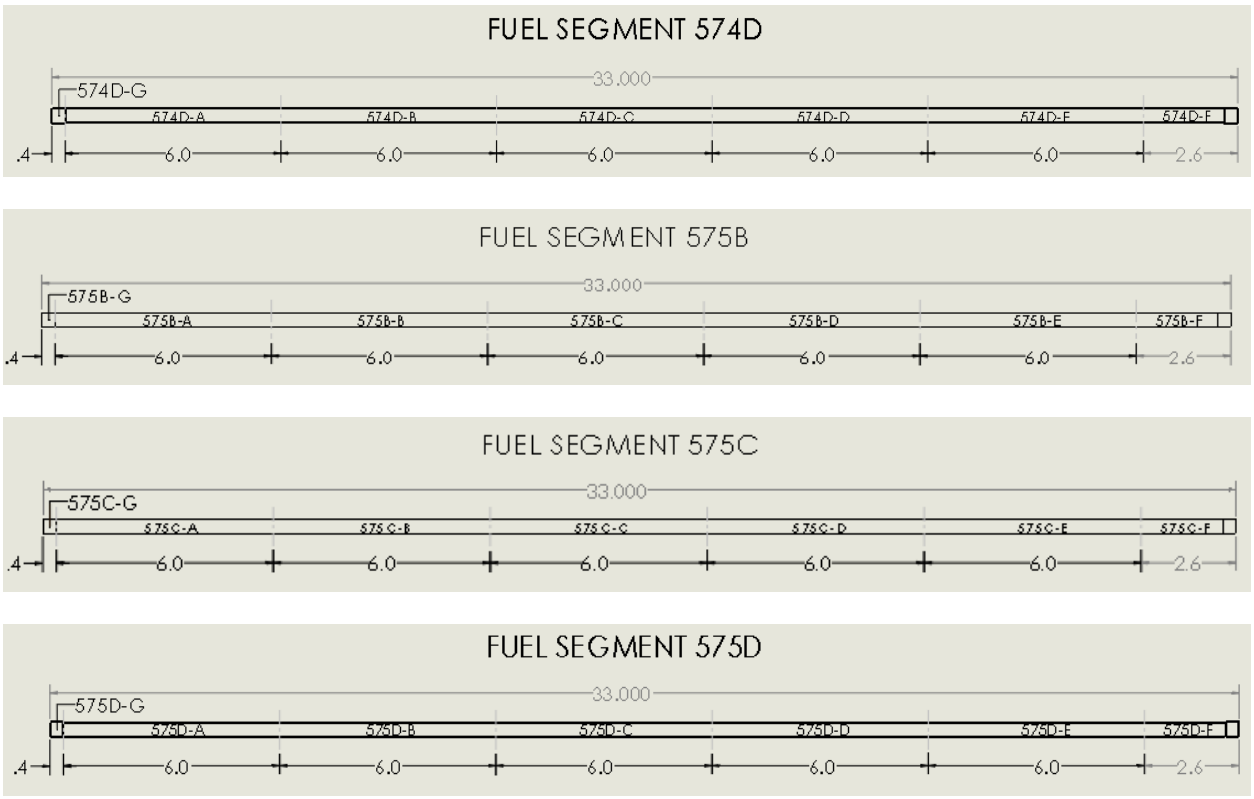

Fig. 1. Cutting plan of BWR Limerick SNF rods for CIRFT testing.[9]

Table 1. Segment identification of Limerick SNF rod[9]

Parent segment	Segment ID	Fuel length (in.)	Notes
574D	574D-G	0.38	Bottom end cap (indicated by scratches on fuel rod)
	574D-A	6.00	
	574D-B	6.00	
	574D-C	6.00	
	574D-D	6.00	
	574D-E	6.00	
	574D-F	3.00	Partial segment and top end cap
575B	575B-G	0.38	Bottom end cap (indicated by scratches on fuel rod)
	575B-A	6.00	
	575B-B	6.00	
	575B-C	6.00	
	575B-D	6.00	
	575B-E	6.00	
	575B-F	3.00	Partial segment and top end cap
575C	575C-G	0.38	Bottom end cap (indicated by scratches on fuel rod)
	575C-A	6.00	
	575C-B	6.00	
	575C-C	6.00	
	575C-D	6.00	
	575C-E	6.00	
	575C-F	3.00	Partial segment and top end cap
575D	575D-G	0.38	Bottom end cap (indicated by scratches on fuel rod)
	575D-A	6.00	
	575D-B	6.00	
	575D-C	6.00	
	575D-D	6.00	
	575D-E	6.00	
	575D-F	3.00	Partial segment and top end cap

Table 2. Outer diameters (ODs) of Limerick SNF rod segments (inches)

		Orientation	Distance (inches) from left end (Fig. 1)			Mean
			2.5	3.0	3.5	
1.1.1.1.1.1.1.1	574D-A	A (0°)	0.45274	0.45210	0.45072	0.45185
		B (90°)	0.44852	0.44764	0.44652	0.44756
		Average				0.44971
1.1.1.1.1.1.1.2	575D-A	A (0°)	0.44824	0.44284	0.44664	0.44591
		B (90°)	0.44828	0.44758	0.44620	0.44735
		Average				0.44663

3. SPECIMEN PREPARATION

Each six-inch rod segment was assembled using two end caps. This was done using the developed vise mold designed for BWR SNF rods with larger ODs. The end cap labels and segment IDs are provided in Table 3.

Table 3. CIRFT test number and segment labels of Limerick SNF rod

Test number	End cap A*	End cap B*	Segment ID	Note	
LMK01	LM1A	LM1B	574D-A		
LMK02	LM2A	LM2B	575D-A		
LMK03	LM3A	LM3B	575B-A		
LMK04	LM4A	LM4B	575B-C	1.1.1.1.1.1.1.3	Two end caps misaligned. Test was not performed on this specimen.
LMK05	LM5A	LM5B	574D-B		
LMK06	LM6A	LM6B	574D-E		
LMK07	LM7A	LM7B	575C-A		
LMK08	LM8A	LM8B	575B-D		
LMK09	LM9A	LM9B	574D-D		
LMK10	LM10A	LM10B	575B-E		
LMK11	LM11A	LM11B	575B-D		
LKM12	LM11A	LM11B	575B-A		

*Rod specimen is loaded into testing machine such that end caps A and B are on motor 2 and motor 1 sides, respectively.

4. STATIC TESTING

4.1 Tuning and Testing Using LMK01/ 574D-A

The testing machine was tuned with specimen LMK01 under displacement control, ±1.0 mm, 5Hz. The tuning parameters were recorded and are shown in Table 4.

Table 4. Tuning parameters based on LMK01

Axial 1		Axial 2	
TuneIQ1	2.080890	TuneIQ1	1.749211
TuneIQ2	0.021591	TuneIQ2	0.017062
TuneIQ3	-10.596725	TuneIQ3	-9.816423

The static test was conducted on LMK01 (574D-A) under a displacement control mode with the test procedure:

1. Initial ramp up to 12.00 mm at 0.1 mm/s rate at each loading point or each Bose motor,
2. Back to 0.0 mm at 0.2 mm/s
3. If the rod specimen does not fail during testing, repeat 1) and 2) two more times

Sample LMK01 survived three loading cycles without any sign of failure. The moment–curvature curves are shown in Fig. 2. There was a significant non-linear deformation after 35 N·m, and the maximum moment at a level of 85 N·m was attained during the initial loading cycle. The subsequent loading cycles did not produce additional deformation, but they introduced a closed hysteresis loop. The maximum curvature under a relative displacement of 24.0 mm at loading points of U-frame (i.e., 12.0 mm at each motor) was approximately 4 m^{-1}.

In order to observe the failure mode of the sample, a dynamic test was carried out under ±25.4 N·m, 5 Hz. The lifetime of the rod (N_f) equaled 9.43×10^3 cycles. The rod ultimately failed in the gage section as shown in Fig. 3.

The segments of tested rod specimens were observed under the hot cell stereomicroscope,[10] and images were taken as shown in Fig. 4. The fracture apparently occurred on the pellet-to-pellet interface. The pellets themselves fractured also, which is believed to be due to irradiation. Scratches can be seen as well, particularly along the longitudinal axis. However, the surface integrity of cladding appears to be generally maintained.

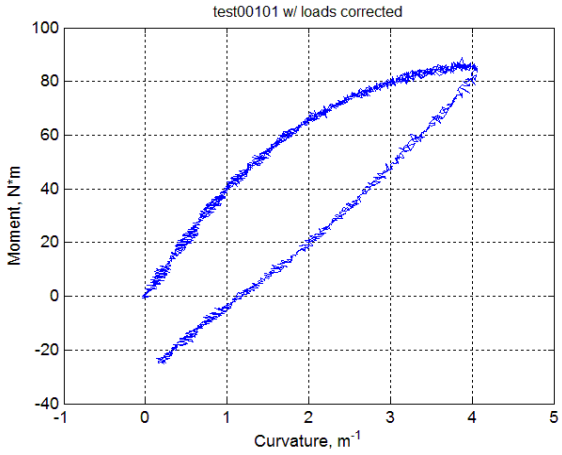

(a)

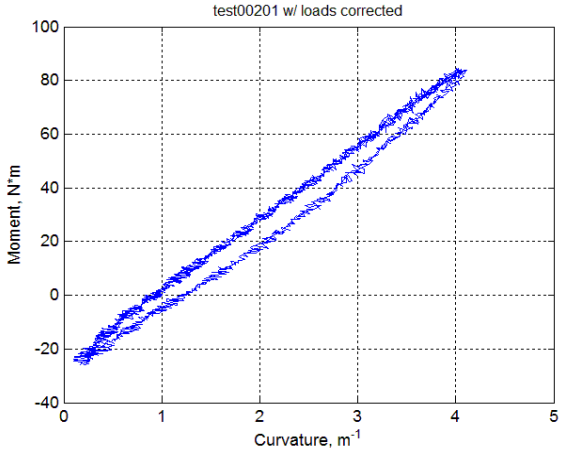

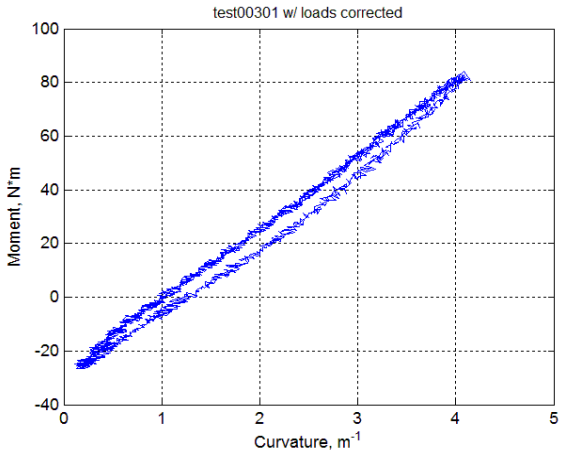

(b)

Fig. 2. Moment-curvature curves in (a) the first loading cycles and (b) the second and third cycles for the LMK01 (574D-A) rod.

Fig. 3. Fracture segments for the LMK01 (574D-A) rod that survived two cycles of loading to relative displacement of 24.00 mm with the maximum moment of around 85 N·m in the initial cycle. A follow-up dynamic test was carried out under ±25.4 N·m, 5 Hz; $N_f = 9.4 \times 10^3$ cycles.

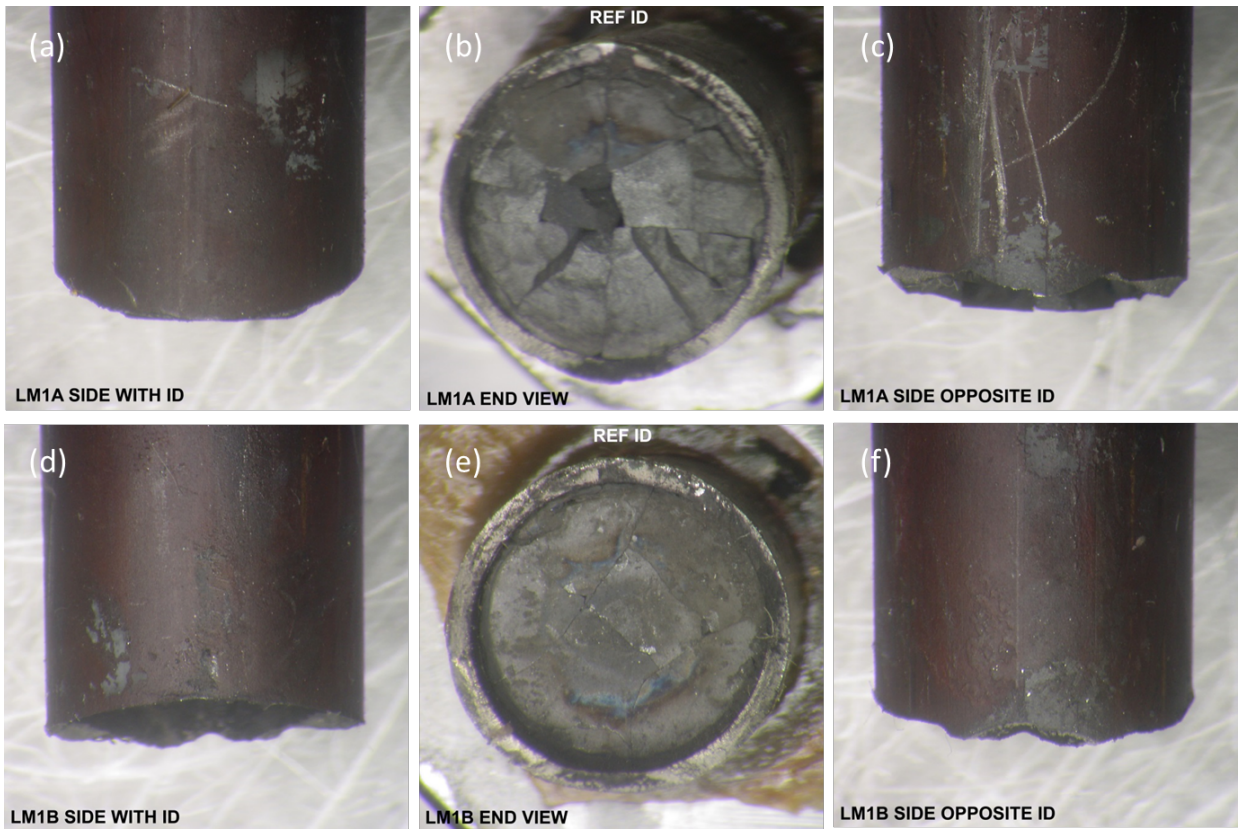

Fig. 4. Fracture segments for LMK01 (574D-A). (a) and (d) show the specimen ID side of the segment on endcaps A and B; (b) and (e) show the mating fracture surface; and (c) and (f) show the opposite specimen ID side of the segment on endcaps A and B.

5. DYNAMIC TESTING

5.1 LMK02/575D-A, ±12.7 N·m, 5Hz

The test on LMK02/575D-A was conducted under ±12.70 N·m, 5 Hz. A lifetime of 1.71×10^5 cycles was obtained. Periodic quasistatic measurements of rod deformation were conducted using two relative displacement levels (0.2, and 0.4 mm) at the selected target number of cycles. The curvature range–moment range and flexural rigidity are illustrated in Fig. 5. The variations of these quantities as a function of number of cycles are further given in Fig. 6. The initial rigidity of the measurements at the two displacements was 47 to 50 $N \cdot m^2$. The rigidity dropped a little near 10^3 cycles, and stayed quite constant after that.

The curvature, moment, and flexural rigidity based on online monitoring data are presented in Fig. 7. The online monitoring showed a flexural rigidity of about 42 $N \cdot m^2$, a little lower than that observed in measurements. This is believed to be because different loading conditions were used in measurement and cycling. A sudden drop of flexural rigidity was observed. Overall, a quite stable response was seen before the final failure. The peak and valley of curvature and moment waveforms were also monitored, as shown in the same figure, and it can be seen that there was no significant offset of curvature during whole fatigue testing

The failure was observed in the gage section again as seen in Fig. 8. The feature of fracture surface is not quite clearly observed at this level of resolution.

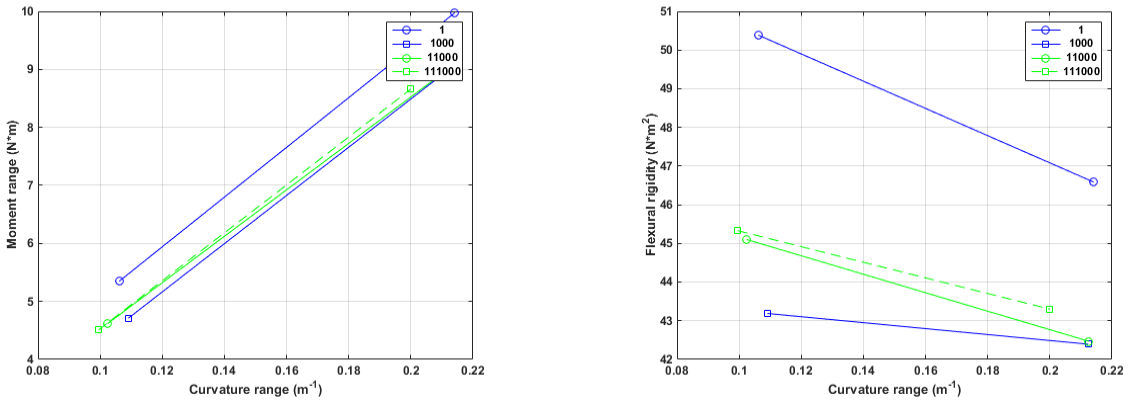

(a) **(b)**

Fig. 5. (a) Moment-curvature relation and (b) moment-flexural rigidity relation at various numbers of cycles for LMK02/575D-A. Measurements were made with 0.2, and 0.4 mm relative displacements; $N_f = 1.71 \times 10^5$ cycles under ±12.70 N·m, 5 Hz.

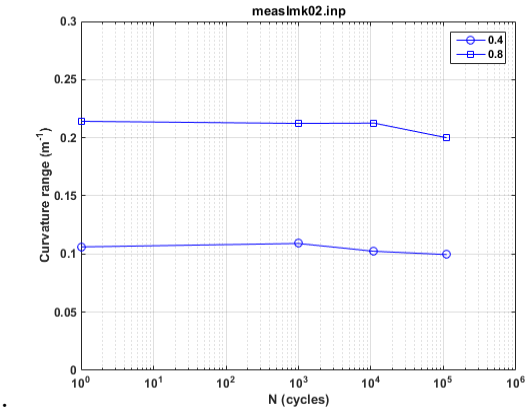

(a)

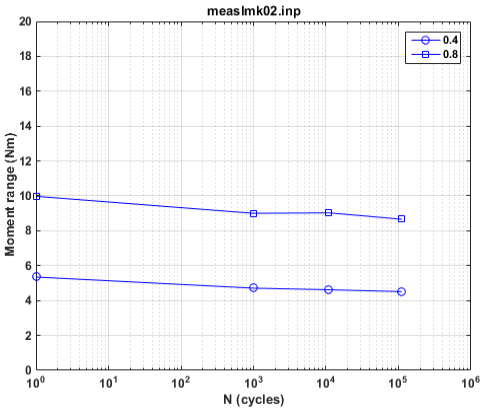

(b)

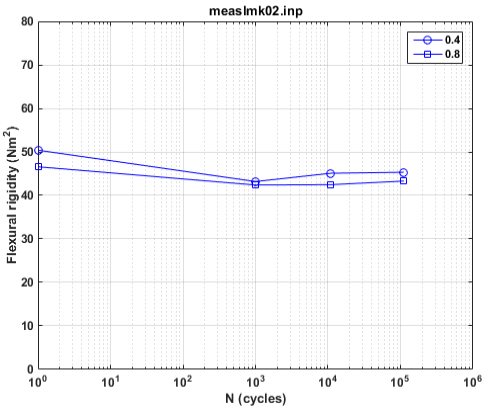

(c)

Fig. 6. Variations of (a) curvature range, (b) moment range, and (c) flexural rigidity as a function of number of cycles for LMK02/575D-A.Measurements were made with 0.2, and 0.4 mm relative displacements; $N_f = 1.71 \times 10^5$ cycles under ±12.70 N·m, 5 Hz.

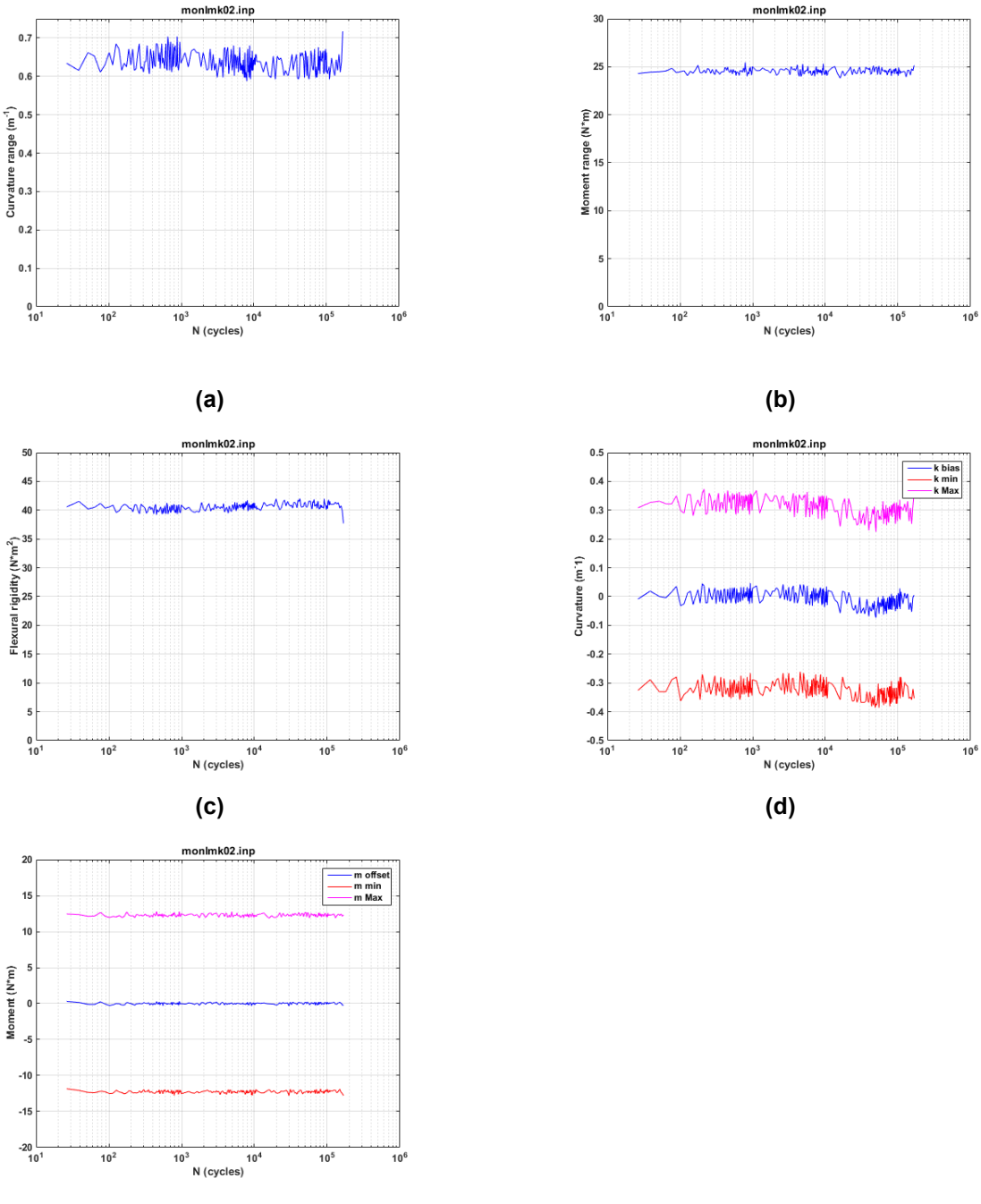

Fig. 7. Variations of (a) curvature range, (b) applied moment range, (c) flexural rigidity, (d) maximum and minimum values of curvature, and (e) maximum and minimum values of moment as a function of number of cycles for LMK02/575D-A; $N_f = 1.71 \times 10^5$ cycles under ±12.70 N·m, 5 Hz.

Fig. 8. Fracture segments for LMK02/575D-A;
$N_f = 1.71 \times 10^5$ cycles under ±12.70 N·m, 5 Hz.

5.2 LMK03/575B-A, ±10.16 Nm, 5Hz

The test on LMK03/575B-A was conducted under ±10.16 N·m, 5 Hz. The applied moment was higher than that of LMK02, and lifetime of the specimen is accordingly longer, 4.92×10^5 cycles.

Periodic quasistatic measurements of rod deformation were conducted using two relative displacement levels (0.2, and 0.4 mm) at the selected target number of cycles. The variations of curvature range, moment range, and flexural rigidity as a function of number of cycles are given in Fig. 9. The rigidity of the measurements at the two displacements started with 44 to 48 N·m^2, dropped to less than 40 N·m^2 around 10^3 cycles, and remained nearly at a constant level afterwards.

The curvature, moment, and flexural rigidity based on online monitoring data are presented in Fig. 10. The online monitoring showed a flexural rigidity of about 35 N·m^2, a little lower than that observed in measurements. Again, an abrupt decrease in flexural rigidity was seen before the final failure.

The failure occurred in the gage section again as seen in Fig. 11. The failed specimen was manually broken into two pieces for fractographic study. The images of lateral surface and fracture surfaces are presented in Fig. 12. Again, the fracture occurred on the pellet-to-pellet interface. Cracks were developed in pellets and pellets fractured into several large size of fragments that were held in place. No apparent gap can be seen between the pellet and cladding. On the specimen ID side, a gray area can be seen. It cannot be seen if the gray area is a damage area at this magnification level.

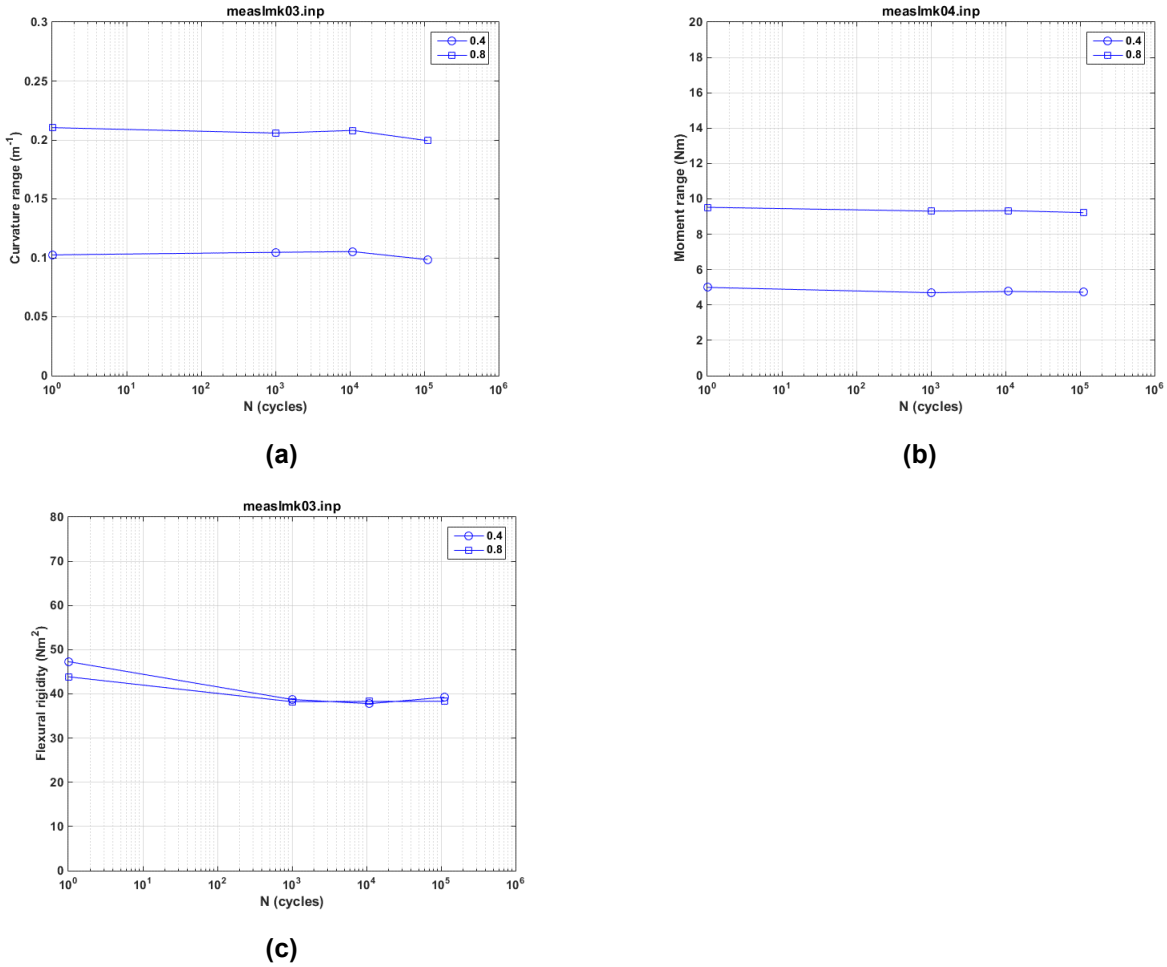

Fig. 9. Variations of (a) curvature range, (b) moment range, and (c) flexural rigidity as a function of number of cycles for LMK03/575B-A; $N_f = 4.92 \times 10^5$ cycles under ±10.16 N·m, 5 Hz.

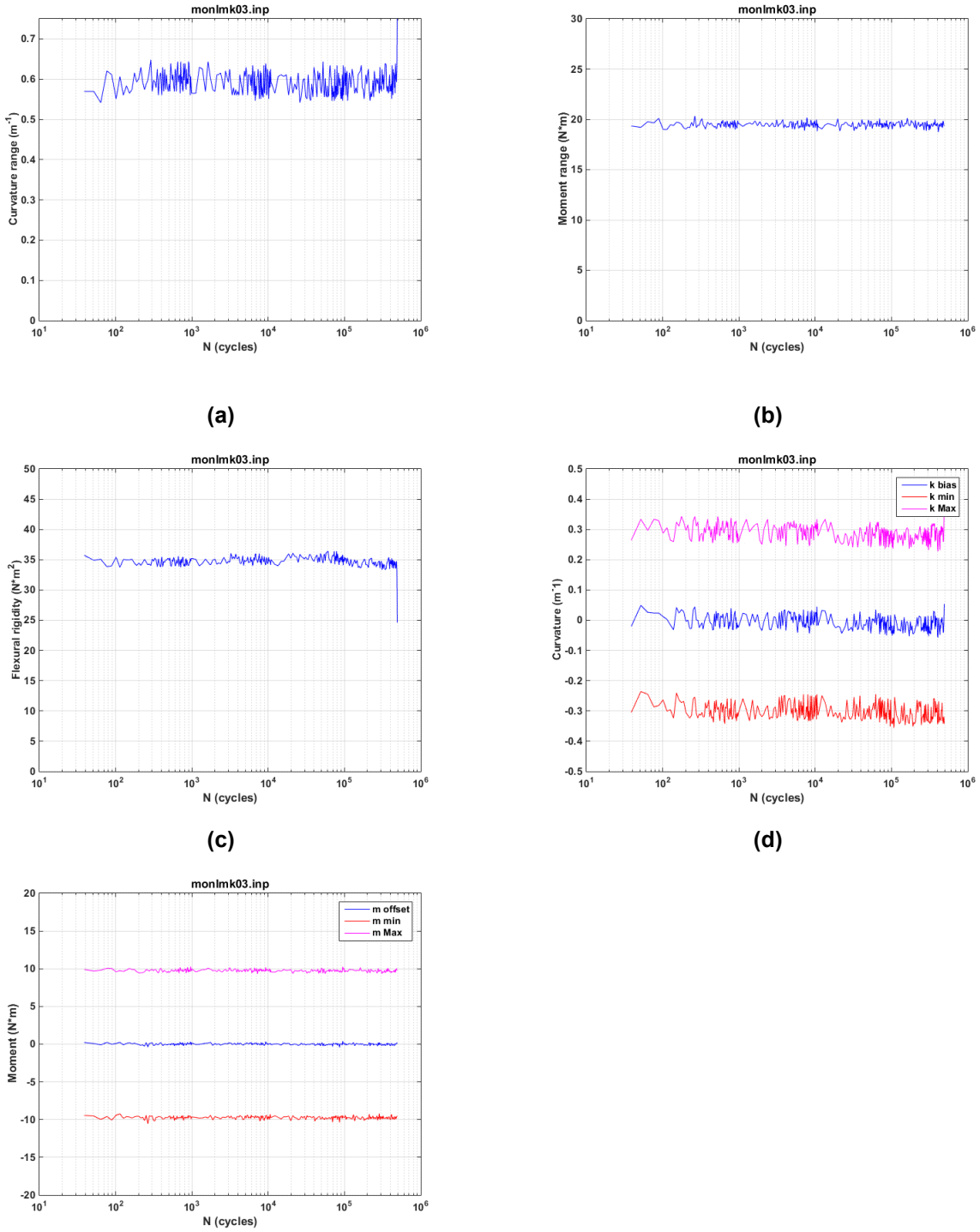

Fig. 10. Variations of (a) curvature range, (b) applied moment range, (c) flexural rigidity, (d) maximum and minimum values of curvature, and (e) maximum and minimum values of moment as a function of number of cycles for LMK03/575B-A; Nf = 4.92 × 105 cycles under ±10.16 N·m, 5 Hz.

Fig. 11. Fracture segments for LMK03/575B-A $N_f = 4.92 \times 10^5$ cycles under ±10.16 N·m, 5 Hz.

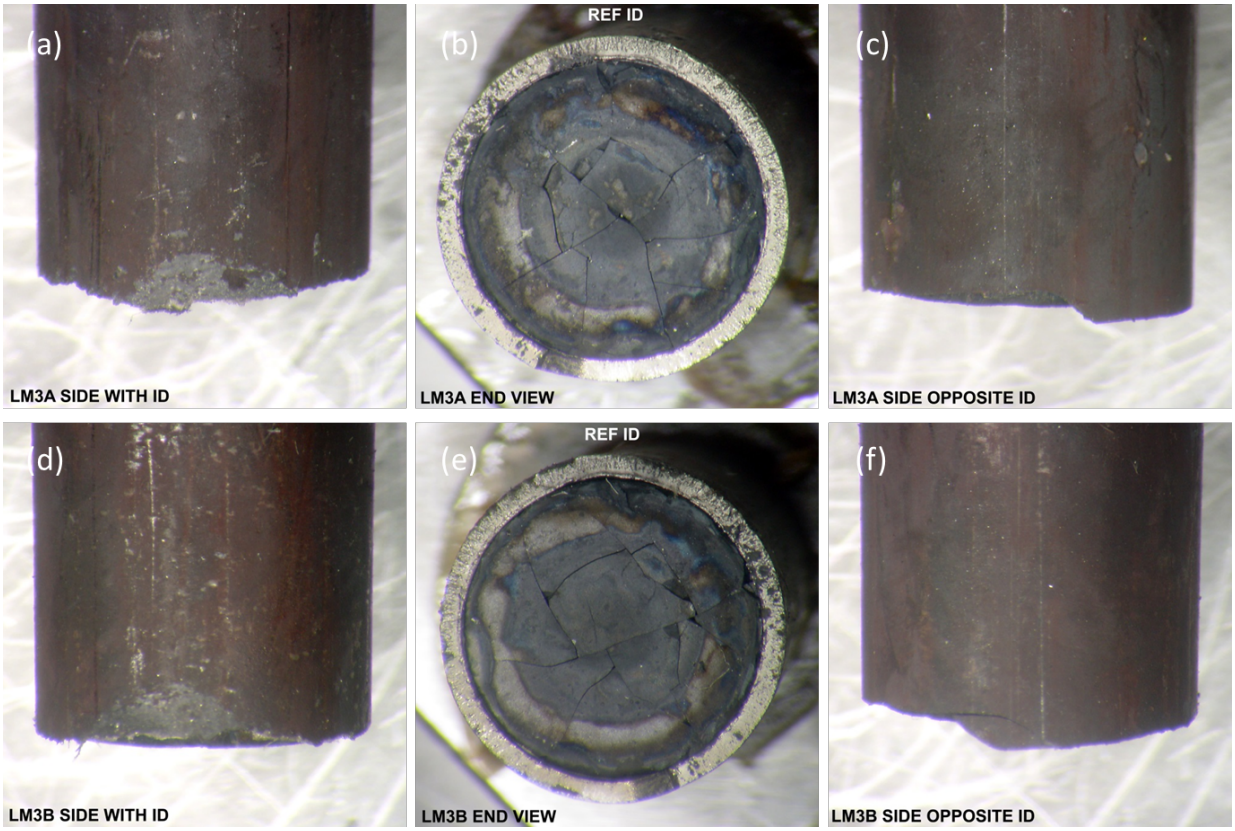

Fig. 12. Fracture segments for LMK03/575B-A. (a) and (d) show the specimen ID side of the segment on endcaps A and B; (b) and (e) show the mating fracture surface; and (c) and (f) show the opposite specimen ID side of segment on endcaps A and B.

5.3 LMK05/574D-B, ±8.64 Nm, 5Hz

The test on the LMK05/574D-B rod was conducted under ±8.64 N·m, 5 Hz. The lifetime of the specimen is 2.49×10^5 cycles. Periodic quasistatic measurements of rod deformation were conducted using two relative displacement levels (0.2, and 0.4 mm) at the selected target number of cycles. The variations of curvature range, moment range, and flexural rigidity as a function of number of cycles are given in Fig. 13. With an initial level of 45 Nm^2, the rigidity of the measurements at the two displacements stayed almost at a constant level over the whole fatigue testing process.

The curvature, moment, and flexural rigidity based on online monitoring data are presented in Fig. 14. The online monitoring showed a flexural rigidity of about 37.5 Nm^2 in most of the testing. An abrupt drop was observed again before the final failure of the specimen. In addition, curvature waveform demonstrated a negative curvature offset of about -0.075 m^{-1}, and drifting at 10^5 cycles. The drift may be related to the tightening of bolts in specimen grips. Compared to LMK03, a shorter lifetime was obtained even though a lower moment amplitude was used. Whether the uncertainty of the testing result is caused by variation of the initial condition of the segment remains to be investigated.

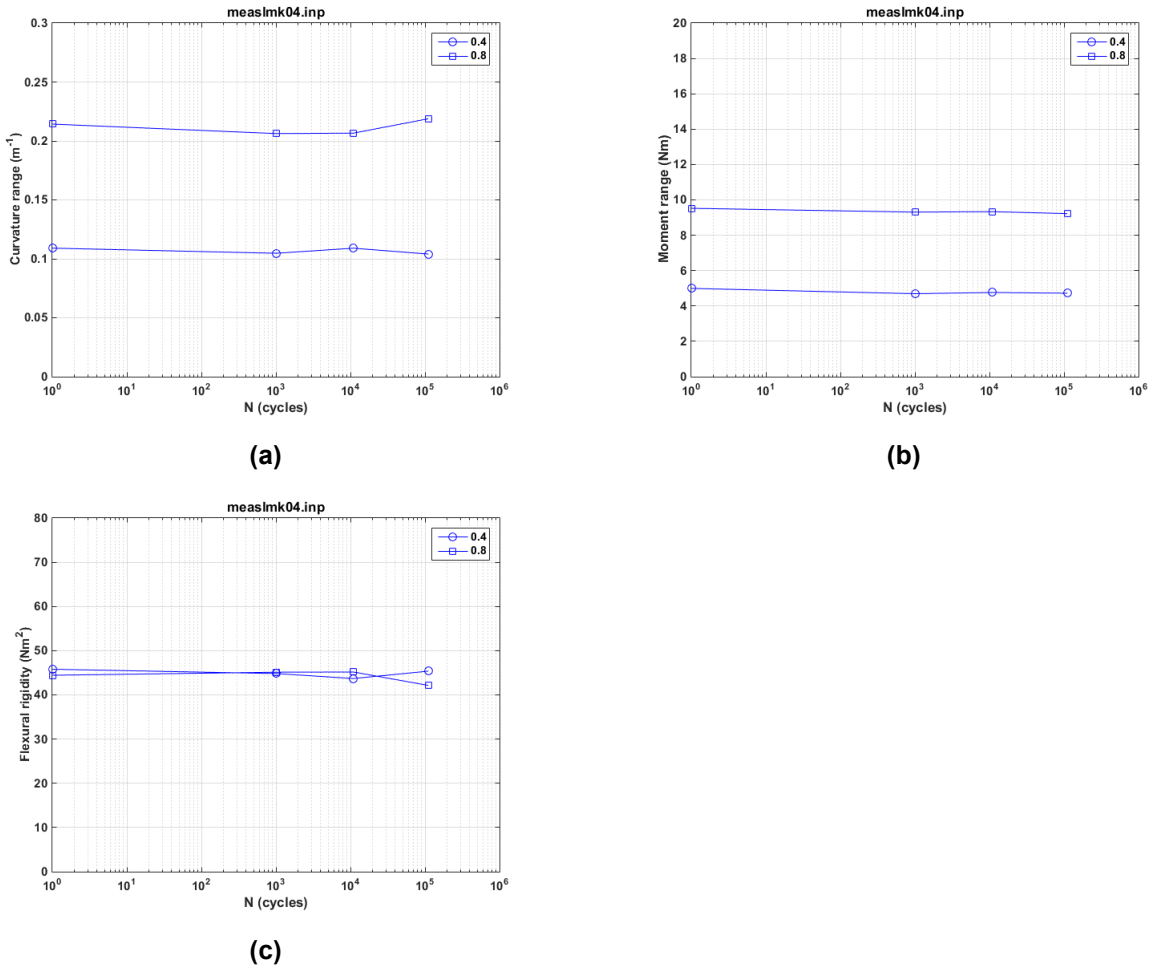

Fig. 13. Variations of (a) curvature range, (b) moment range, and (c) flexural rigidity as a function of number of cycles for LMK05/574D-B; $N_f = 2.49 \times 10^5$ cycles under ±8.64 N·m, 5 Hz.

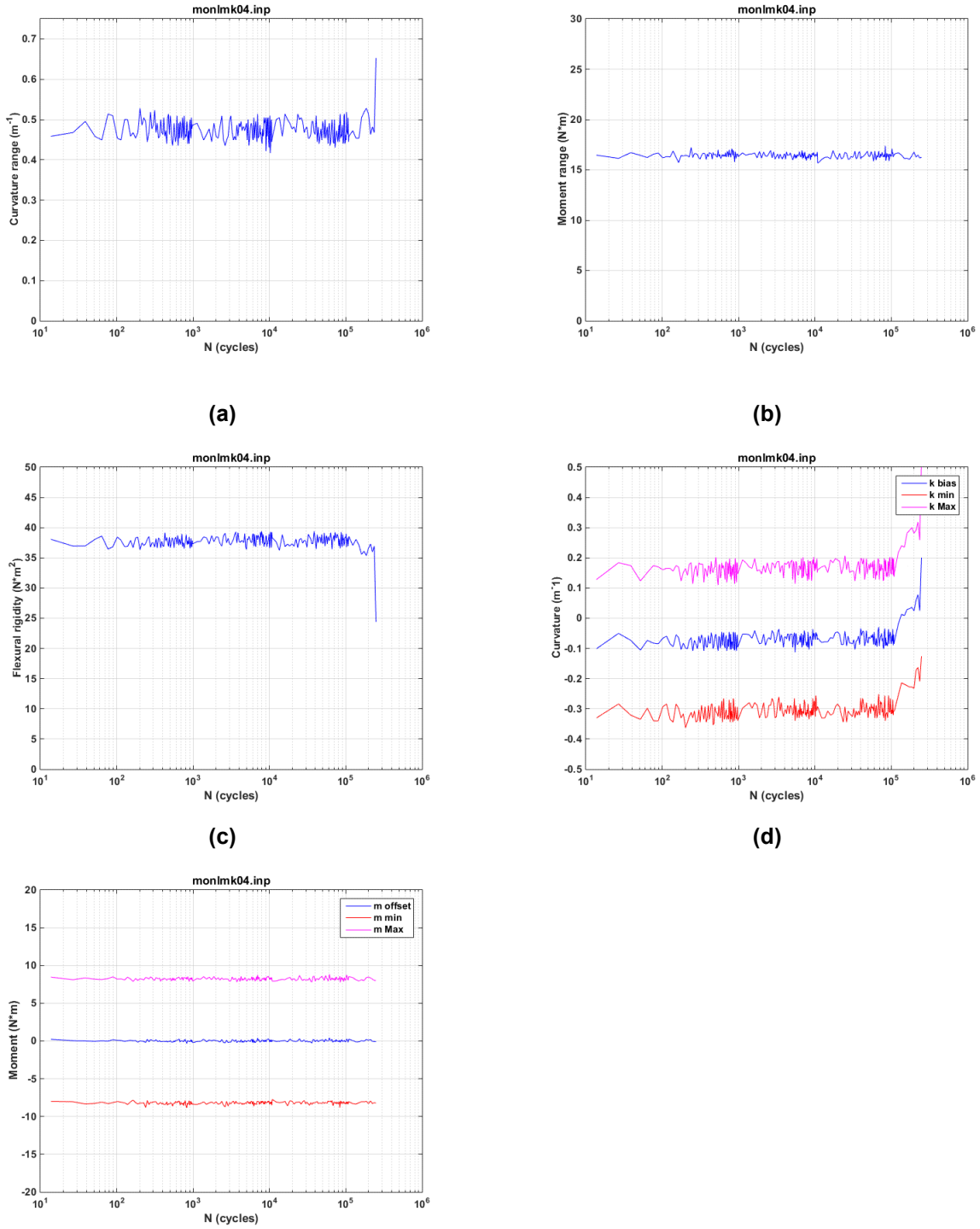

Fig. 14. Variations of (a) curvature range, (b) applied moment range, (c) flexural rigidity, (d) maximum and minimum values of curvature, and (e) maximum and minimum values of moment as a function of number of cycles for LMK05/574D-B; $N_f = 2.49 \times 10^5$ cycles under ±8.64 N·m, 5 Hz.

5.4 LMK06/574D-E, ±7.62 Nm, 5Hz

The test on the LMK06/575D-E rod was conducted under ±7.62 N·m, 5 Hz. The lifetime of the specimen is 1.79×10^6 cycles. Periodic quasistatic measurements of rod deformation were conducted using two relative displacement levels (0.2, and 0.35 mm) at the selected target number of cycles. The variations of curvature range, moment range, and flexural rigidity as a function of the number of cycles are given in Fig. 15. The rigidity of the measurements was observed to be fluctuating a little, but it essentially stayed around 42 Nm^2 during the cyclic testing.

The curvature, moment, and flexural rigidity based on online monitoring data are presented in Fig. 16. The online monitoring showed a flexural rigidity of about 33 Nm^2, a little lower than that observed in measurements. Overall, a quite stable rod response was exhibited before the final failure. At the same time, a negative curvature offset of approximately -0.075 m^{-1} was observed from the peak and valley monitoring of waveform.

The examination of the tested specimen indicated that the failure is located inside of one end cap. It is not certain if out-of-gage section failure is related to the structural flaw or the epoxy casting of the end cap. Nevertheless, among all the dynamic tests that were completed (LMK02, 03, 05 and 06), a longer lifetime was obtained with LMK06 when a lower moment amplitude was used.

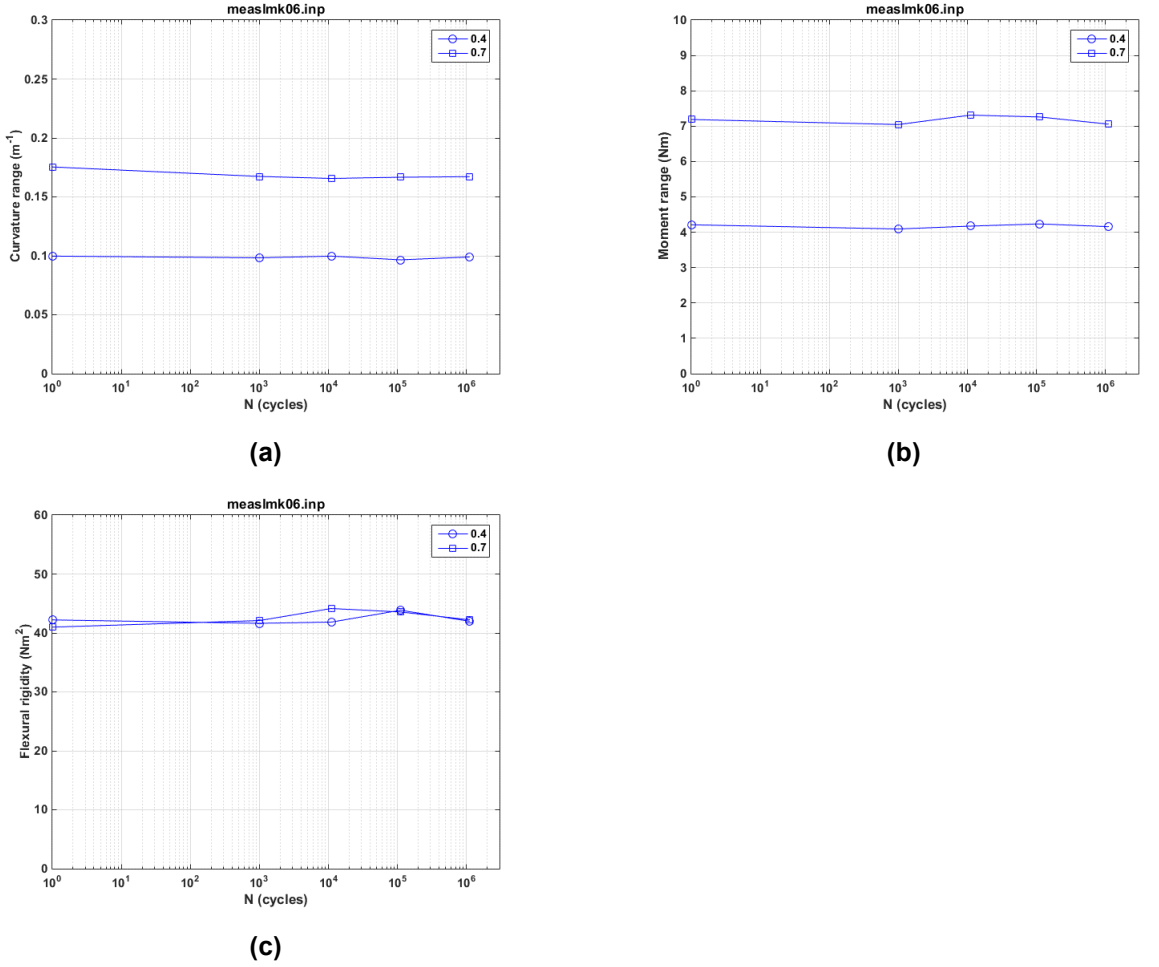

Fig. 15. Variations of (a) curvature range, (b) moment range, and (c) flexural rigidity as a function of number of cycles for LMK06/575D-E; $N_f = 1.79 \times 10^6$ cycles under ±7.62 N·m, 5 Hz.

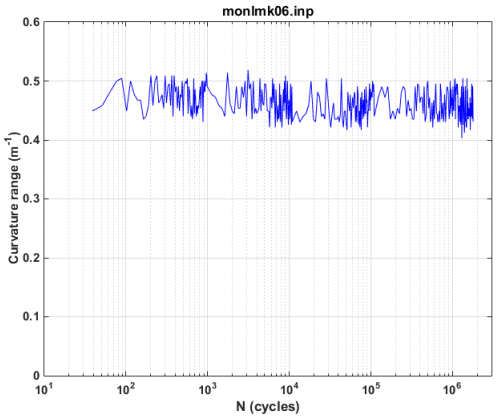

(a)

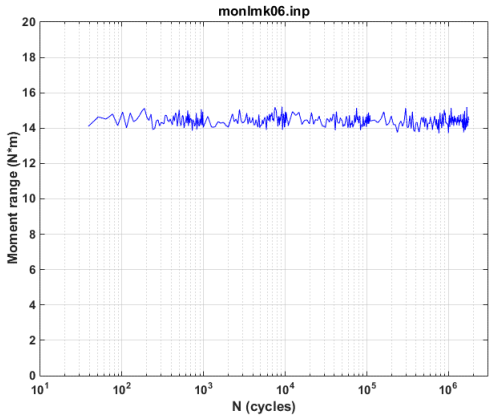

(b)

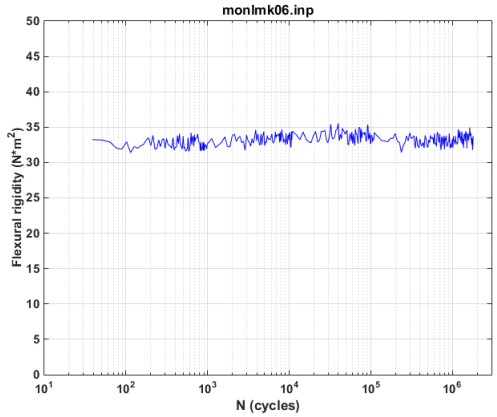

(c)

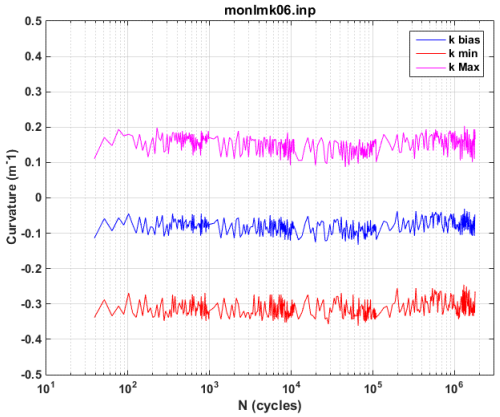

(d)

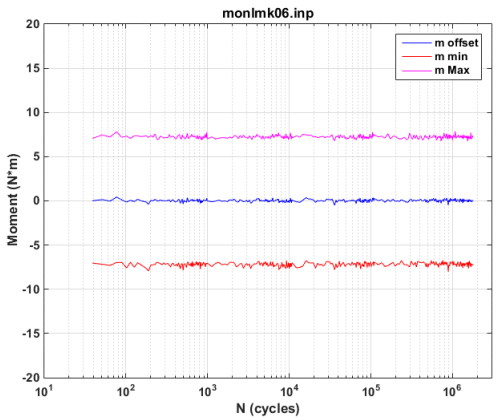

(e)

Fig. 16. Variations of (a) curvature range, (b) applied moment range, (c) flexural rigidity, (d) maximum and minimum values of curvature, and (e) maximum and minimum values of moment as a function of number of cycles for LMK06/575D-E; Nf = 1.79 × 106 cycles under ±7.62 N·m, 5 Hz.

5.5 LMK07/575C-A, ±15.24 Nm, 5Hz

The test on the LMK07/575C-A rod was conducted under ±15.24 N·m, 5 Hz. The lifetime of the specimen is 1.22×10^5 cycles. Periodic quasistatic measurements of rod deformation were conducted using two relative displacement levels (0.2, and 0.4 mm) at the selected target number of cycles. The variations of curvature range, moment range, and flexural rigidity as a function of number of cycles are given in Fig. 17. As can be seen, there was a significant decrease in rigidity near 10^5 cycles from 45–50 to ~40 Nm^2, corresponding to the high moment cycling.

The curvature, moment, and flexural rigidity based on online monitoring data are presented in Fig. 18. The online monitoring showed a flexural rigidity of about 38 Nm^2, a little lower than that observed in measurements. Essentially, no significant change can be observed with the monitored flexural rigidity over the cyclic testing process, except a little bend down of curve near 7×10^4 cycles. At the same time, a little negative curvature offset (-0.05 m^{-1}) was observed.

The images of lateral surface and fracture surfaces are presented in Fig. 19. The feature of fracture surface is quite similar to that observed in LMK03. Again, the fracture occurred on the pellet-to-pellet interface. Cracks were developed in pellets, and pellets fractured into several large size fragments but they held in place. There seemed to be filling on the pellet-to-cladding interface, but it cannot be identified at this level of magnification.

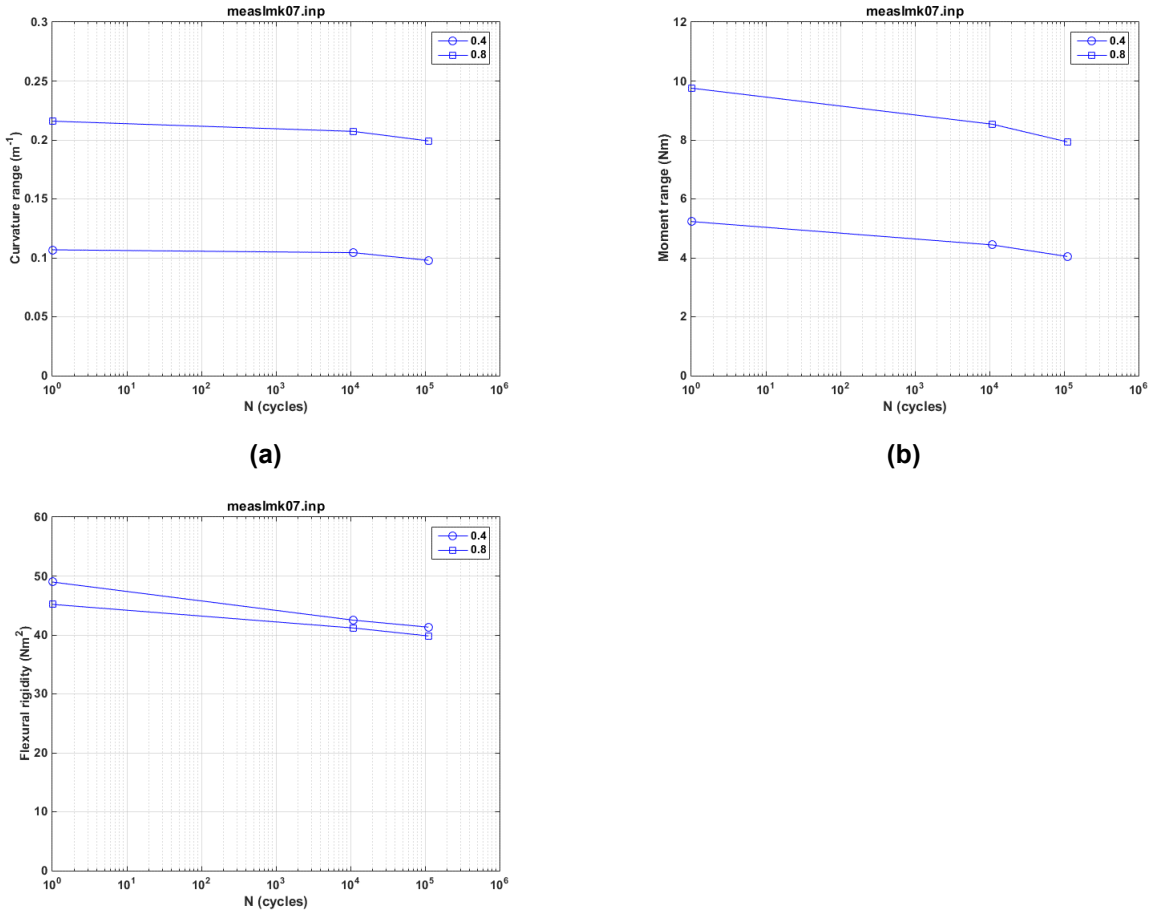

Fig. 17. Variations of (a) curvature range, (b) moment range, and (c) flexural rigidity as a function of number of cycles for LMK07/575C-A; $N_f = 1.22 \times 10^5$ cycles under ±15.24 N·m, 5 Hz.

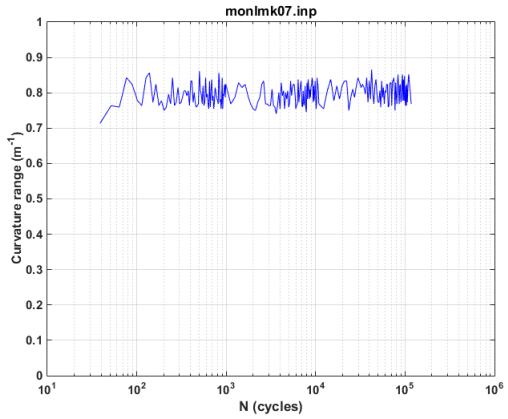

(a)

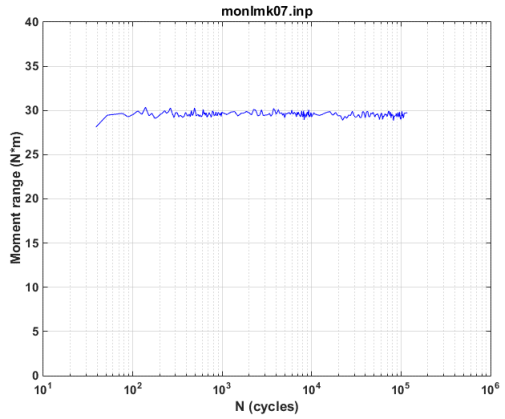

(b)

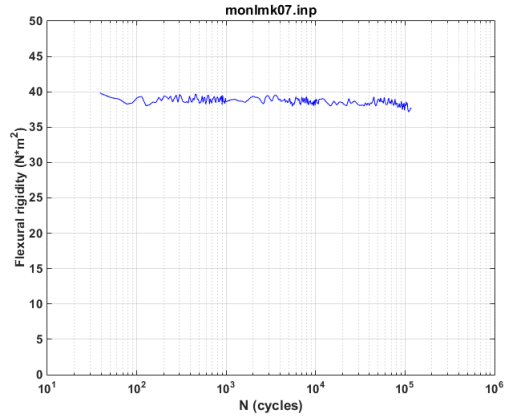

(c)

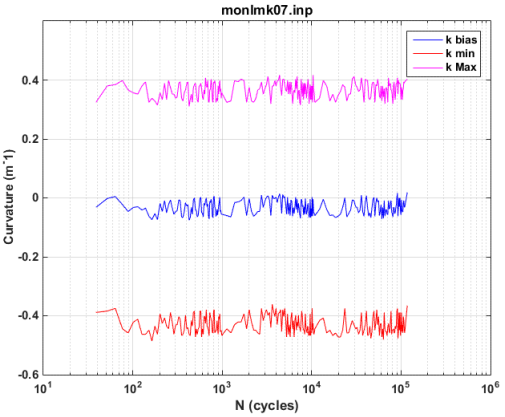

(d)

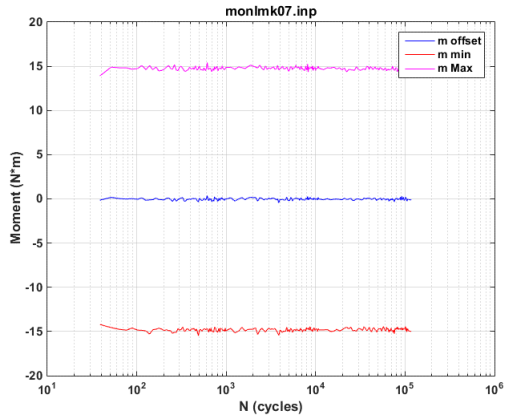

(e)

Fig. 18. Variations of (a) curvature range, (b) applied moment range, (c) flexural rigidity, (d) maximum and minimum values of curvature, and (e) maximum and minimum values of moment as a function of number of cycles for LMK07/575C-A; $N_f = 1.22 \times 10^5$ cycles under ±15.24 N·m, 5 Hz.

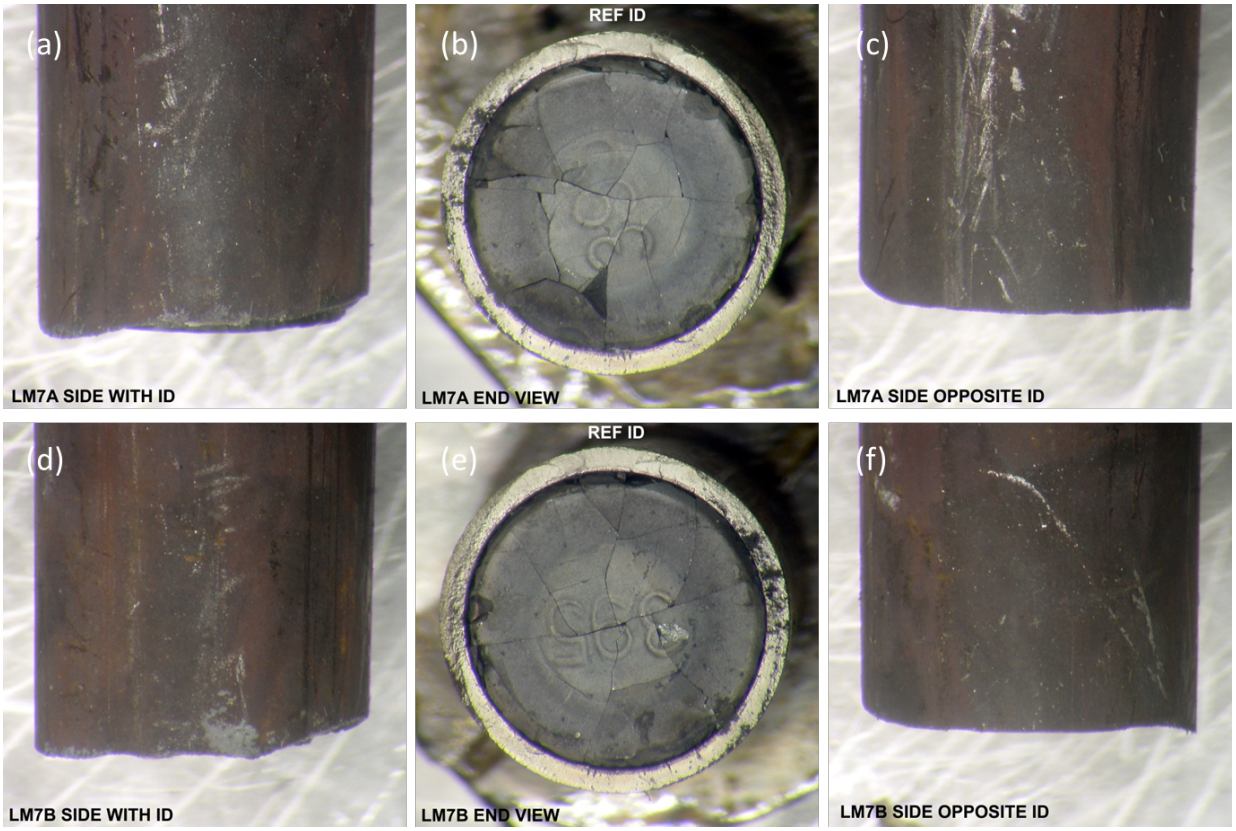

Fig. 19. Fracture segments for LMK07/575C-A. (a) and (d) show the specimen ID side of the segments on endcaps A and B; (b) and (e) show the mating fracture surface; and (c) and (f) show the opposite specimen ID side of segment on endcaps A and B.

5.6 LMK08/575B-D, ±7.62N·m, 5Hz

The test on the LMK08/575B-D rod was conducted under ±7.62 N·m, 5 Hz. The specimen failed at 4.70×10^6 cycles. Periodic quasi static measurements of rod deformation were conducted using two relative displacement levels (0.2, and 0.35 mm) at the selected target number of cycles. The variations of curvature range, moment range, and flexural rigidity as a function of number of cycles are given in Fig. 20. The rigidity of the measurements at two displacements started with 43 to 47 Nm^2 and demonstrated a slight decreasing trend.

The curvature, moment, and flexural rigidity based on online monitoring data are presented in Fig. 21. The online monitoring showed a flexural rigidity of about 36.5 Nm^2, a little lower than that observed in measurements. This is mainly because different loading conditions were used in measurement and cycling. Overall, a quite steady response was exhibited over the whole cyclic testing period. Meanwhile, a positive curvature offset of 0.1 m^{-1} was seen during the cyclic fatigue process.

The failure of specimen occurred in the gage section as shown in Fig. 22.

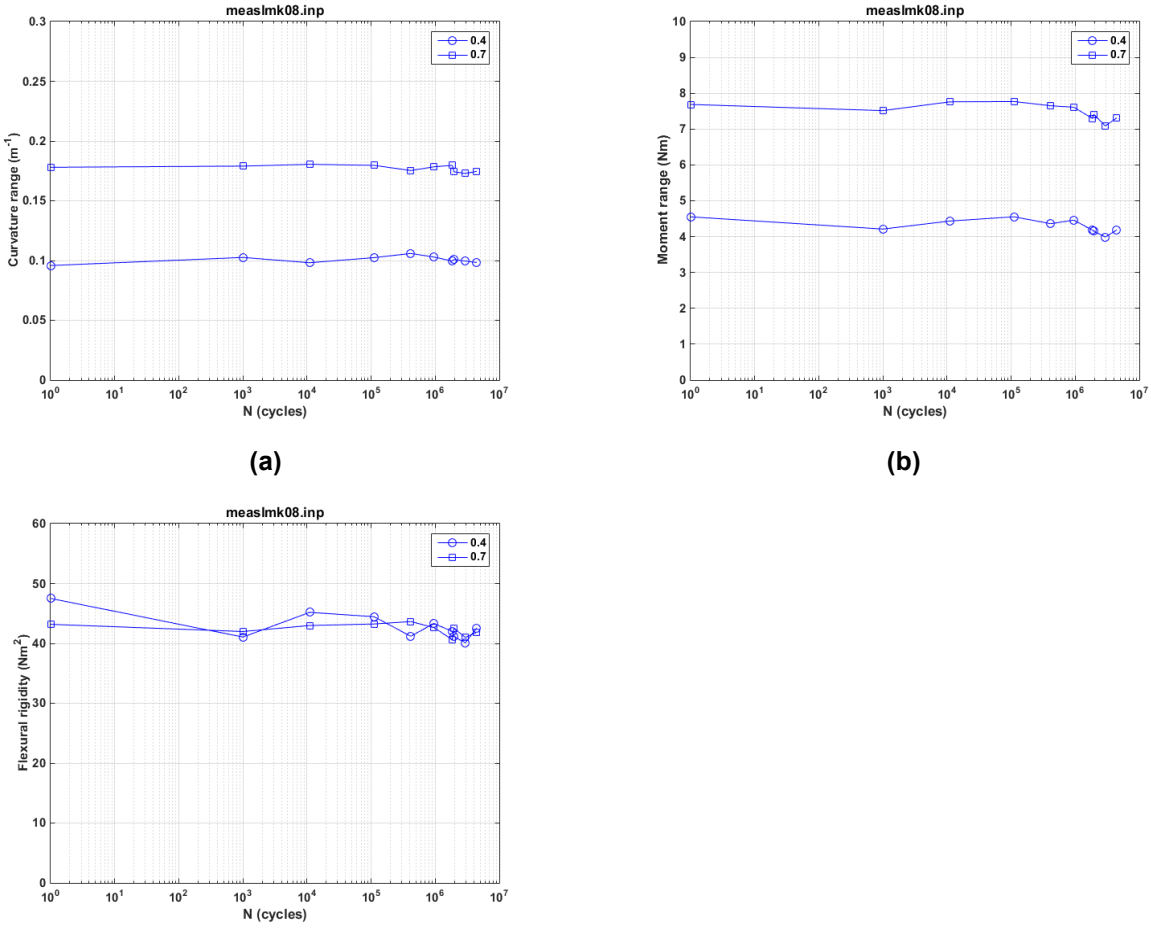

Fig. 20. Variations of (a) curvature range, (b) moment range, and (c) flexural rigidity as a function of number of cycles for LMK08/575B-D. Measurements were made with 0.2, and 0.35 mm relative displacements; $N_f = 4.70 \times 10^6$ cycles under ±7.62 N·m, 5 Hz.

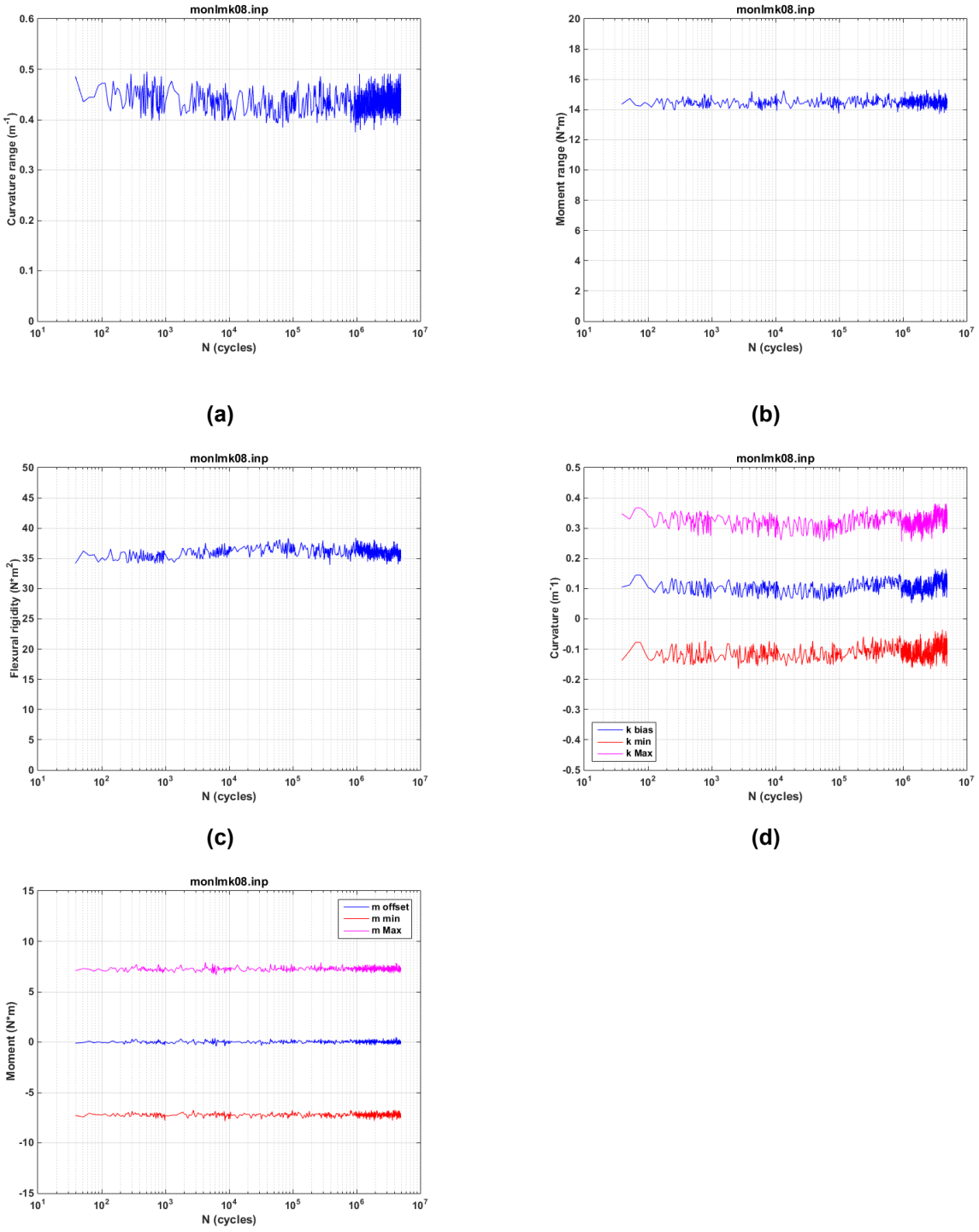

Fig. 21. Variations of (a) curvature range, (b) applied moment range, (c) flexural rigidity, (d) maximum and minimum values of curvature, and (e) maximum and minimum values of moment as a function of number of cycles for LMK08/575B-D; $N_f = 4.70 \times 10^6$ cycles under ±7.62 N·m, 5 Hz.

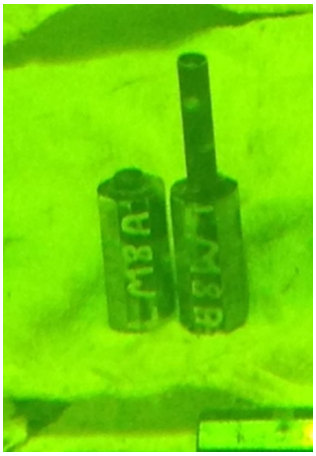

Fig. 22. Fracture segments for LMK08/575B-D; $N_f = 4.70 \times 10^6$ cycles under ±7.62 N·m, 5 Hz.

5.7 LMK09/574D-D, ±10.16N·m, 5Hz

The test on the LMK09/574D-D rod was conducted under ±10.16 N·m, 5 Hz. The specimen failed at 7.31 × 10^5 cycles. Periodic quasistatic measurements of rod deformation were conducted using two relative displacement levels (0.2, and 0.4 mm) at the selected target number of cycles. The variations of curvature range, moment range, and flexural rigidity as a function of number of cycles are given in Fig. 23. The rigidity of the measurements at two displacements started with 45 to 47 Nm^2 and demonstrated a slight decreasing trend.

The curvature, moment, and flexural rigidity based on online monitoring data are presented in Fig. 24. The online monitoring showed a flexural rigidity of about 39 Nm^2, a little lower than that observed in measurements. This is believed to be because different loading conditions were used in measurement and cycling. Overall, a quite steady response was exhibited over the whole cyclic testing period. Meanwhile, a positive curvature offset of 0.02 m^{-1} was seen during the cyclic fatigue process.

The failure occurred again in the middle of gage section of specimen as shown in Fig. 25. Fractographic study was conducted by using stereo-optical microscope. The images of lateral surface and fracture surfaces are presented in 26. Overall surface integrity was maintained to a certain extent. Again, the fracture clearly occurred on the pellet-to-pellet interface. Cracks were developed in pellets and pellets fractured into several large size of fragments that were held in place. No apparent gap can be seen between pellet and cladding.

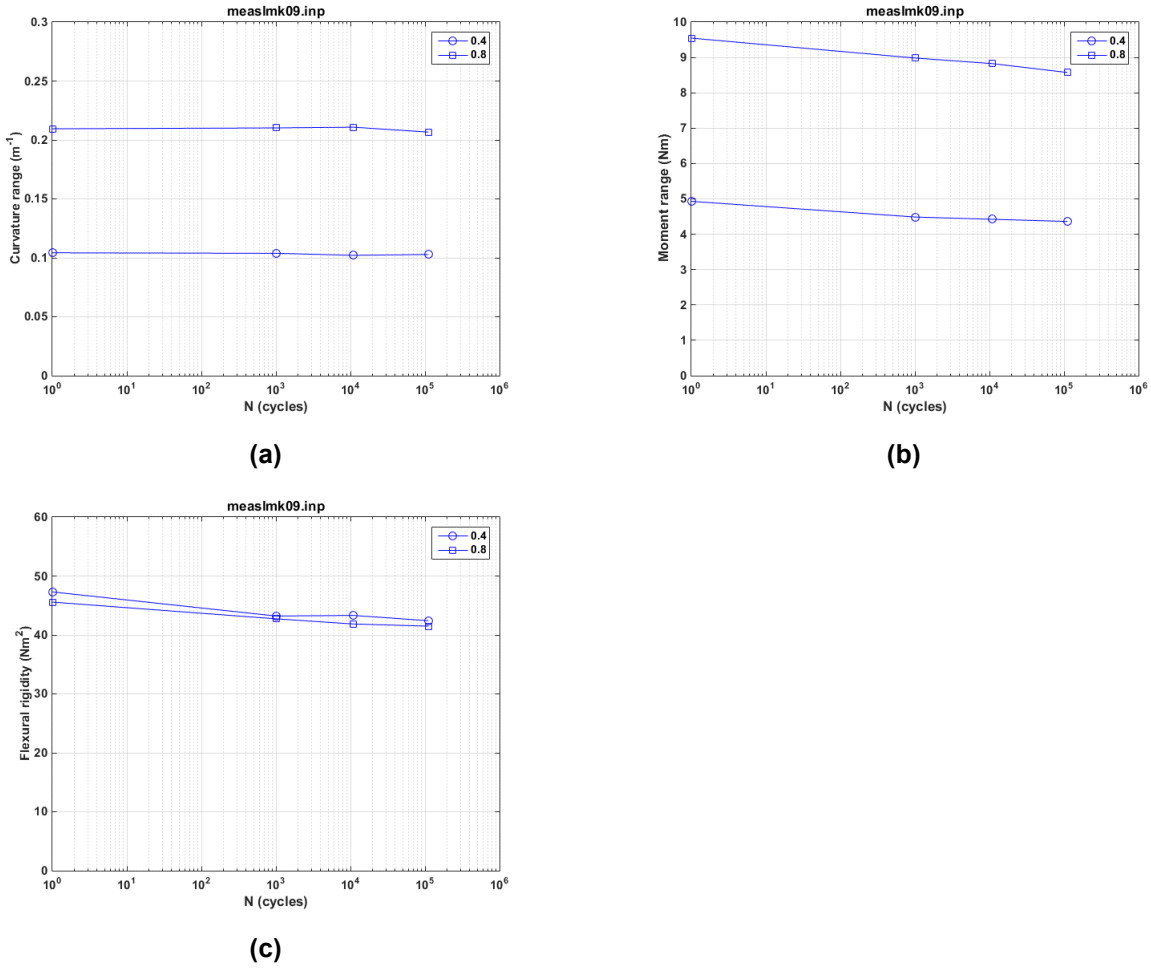

Fig. 23. Variations of (a) curvature range, (b) moment range, (c) flexural rigidity as a function of number of cycles for LMK09/574D-D.Measurements were made with 0.2, and 0.4 mm relative displacements; $N_f = 7.31\times10^5$cycles under ±10.16 N·m, 5 Hz.

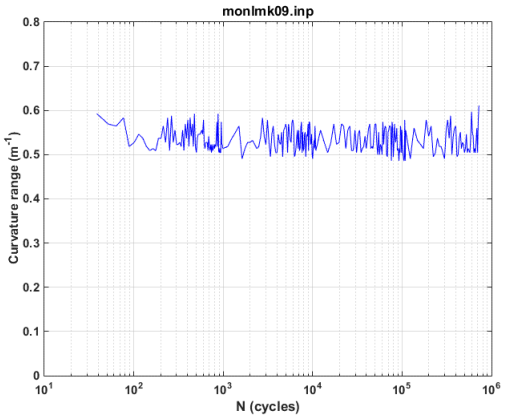

(a)

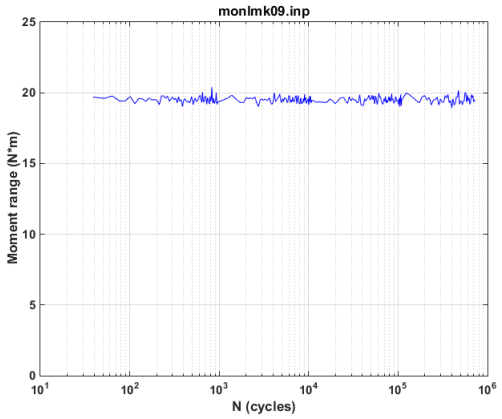

(b)

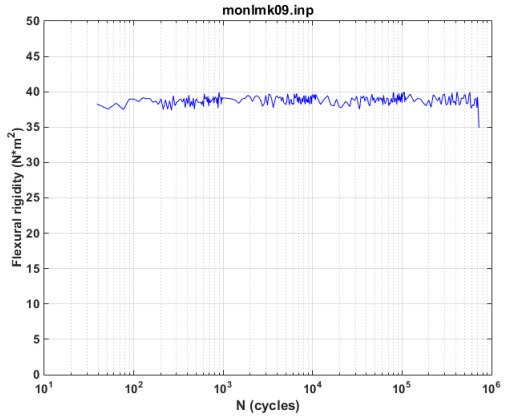

(c)

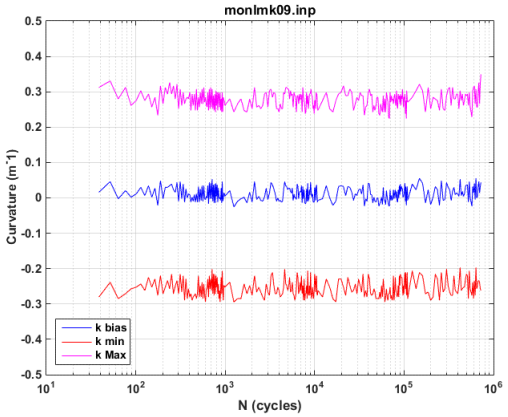

(d)

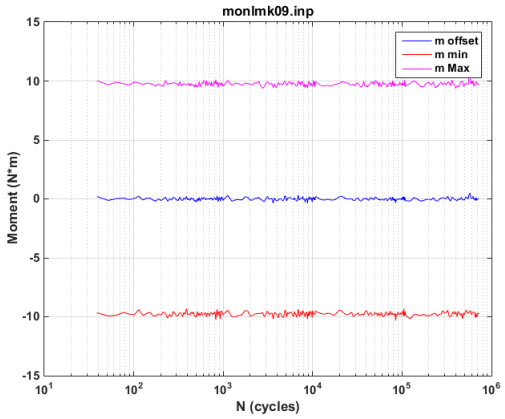

(e)

Fig. 24. Variations of (a) curvature range, (b) applied moment range, (c) flexural rigidity, (d) maximum and minimum values of curvature, and (e) maximum and minimum values of moment as a function of number of cycles for LMK09/574D-D; $N_f = 7.31 \times 10^5$ cycles under ±10.16 N·m, 5 Hz.

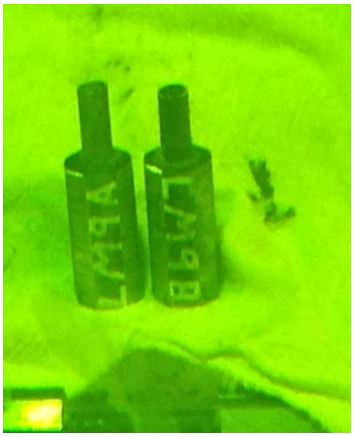

Fig. 25. Fracture segments for LMK09/574D-D; $N_f = 7.31 \times 10^5$ cycles under ±10.16 N·m, 5 Hz.

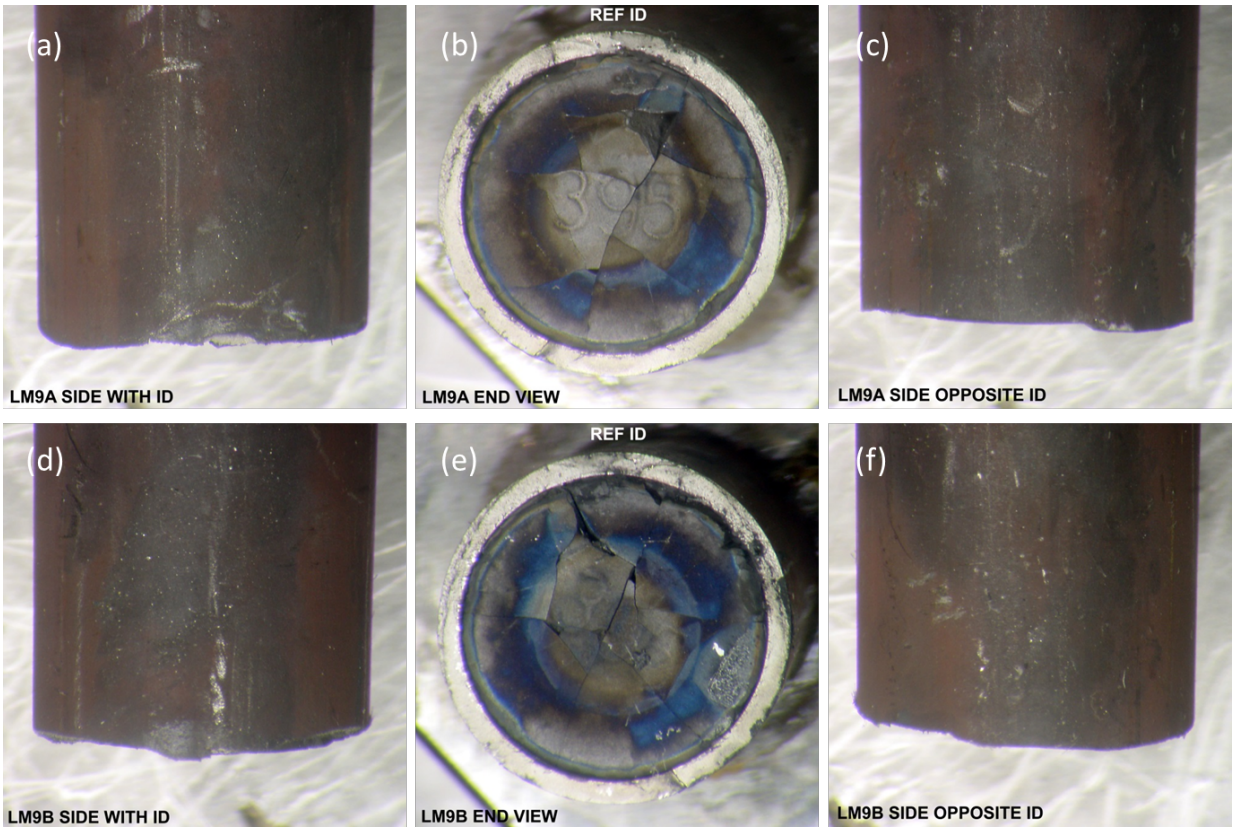

26. Fracture segments for LMK09/574D-D. (a) and (d) show the specimen ID side of the segment on endcaps A and B; (b) and (e) show the mating fracture surface, and (c) and (f) show the opposite specimen ID side of segment on endcaps A and B.

5.8 LMK10/575B-E, ±20.32N·m, 5Hz

The test on the LMK10/575B-E rod was conducted under ±20.32 N·m, 5 Hz. The specimen failed at 5.20×10^4 cycles. Periodic quasistatic measurements of rod deformation were conducted using two relative displacement levels (0.2, and 0.4 mm) at the selected target number of cycles. The variations of curvature range, moment range, and flexural rigidity as a function of number of cycles are given in Fig. 27. The rigidity of the measurements at two displacements started with 45 to 50 Nm^2 and demonstrated a clear decreasing trend.

The curvature, moment, and flexural rigidity based on online monitoring data are presented in Fig. 28. The online monitoring showed a flexural rigidity of about 38 Nm^2, a little lower than that observed in measurements. This is mainly because different loading conditions were used in measurement and cycling. Overall, a quite steady response was exhibited over the whole cyclic testing period. Meanwhile, a positive curvature offset of 0.05 m^{-1} was seen during the cyclic fatigue process.

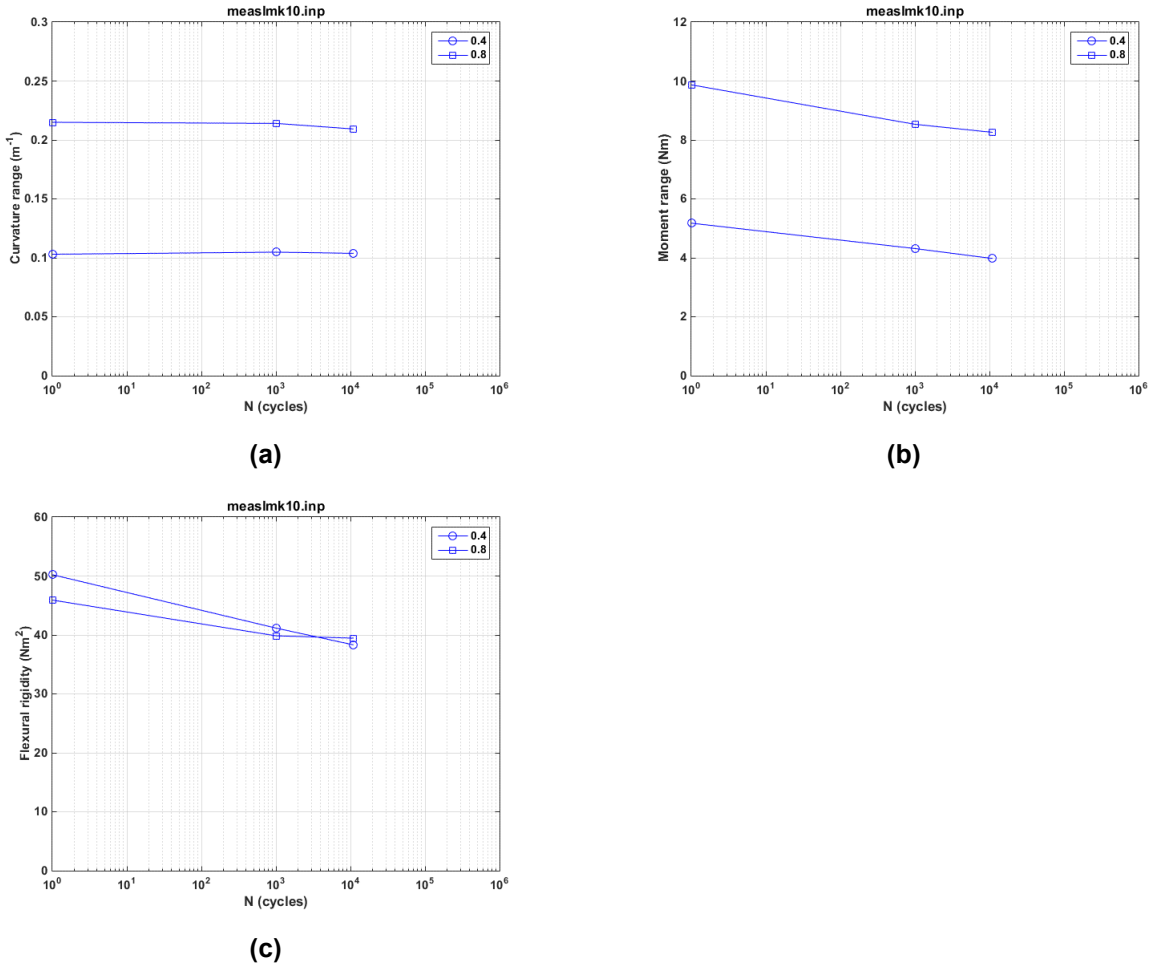

Fig. 27. Variations of (a) curvature range, (b) moment range, and (c) flexural rigidity as a function of number of cycles for LMK10/575B-E. Measurements were made with 0.2, and 0.4 mm relative displacements; $N_f = 5.20 \times 10^4$ cycles under ±20.32 N·m, 5 Hz.

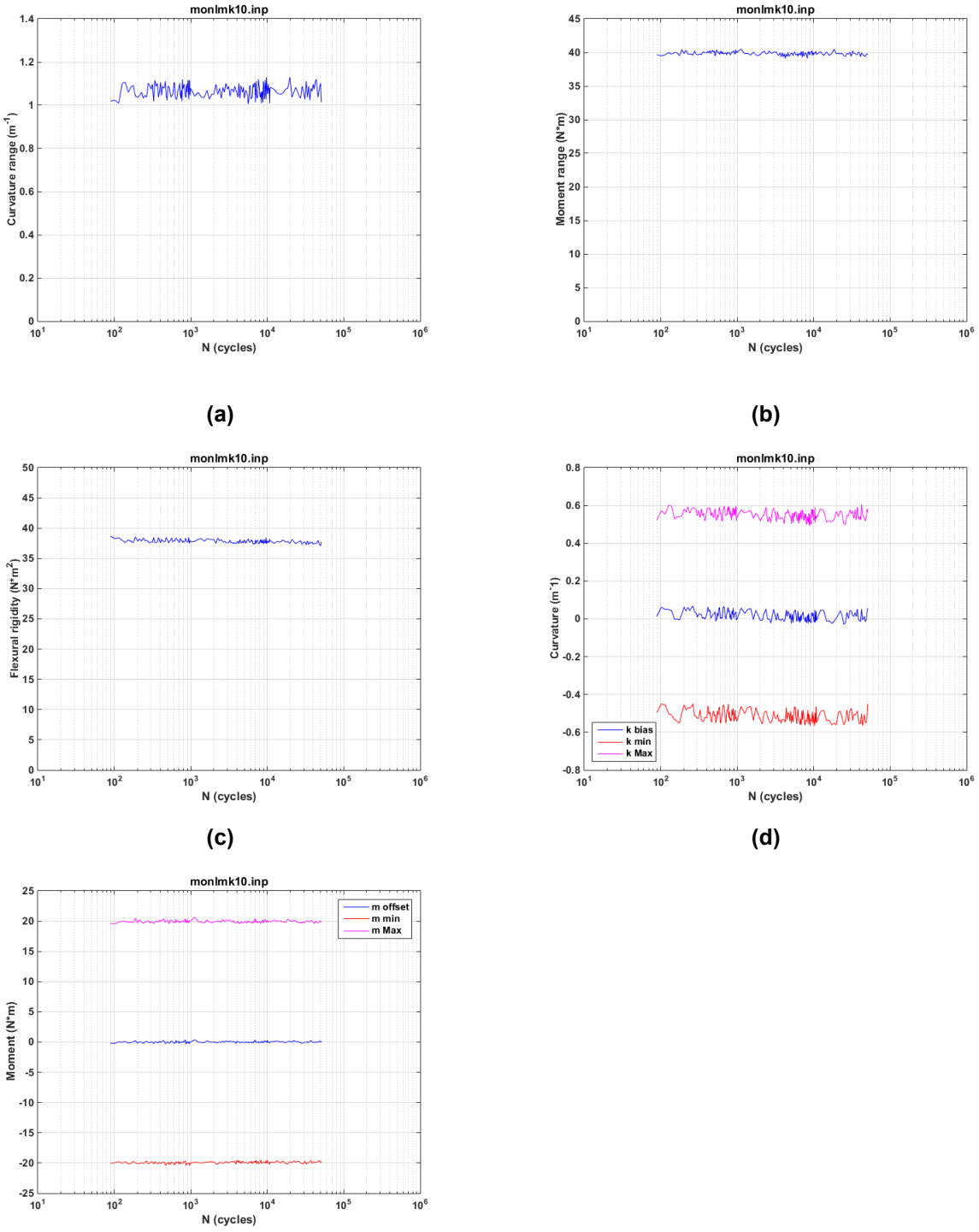

Fig. 28. Variations of (a) curvature range, (b) applied moment range, (c) flexural rigidity, (d) maximum and minimum values of curvature, and (e) maximum and minimum values of moment as a function of number of cycles for LMK10/575B-E; $N_f = 5.20 \times 10^4$ cycles under ±20.32 N·m, 5 Hz.

5.9 LMK11/575B-D, ±8.64N·m, 5Hz

The test on the LMK11/575B-D rod was conducted under ±8.64 N·m, 5 Hz. The specimen failed at 3.55×10^5 cycles. Periodic quasistatic measurements of rod deformation were conducted using two relative displacement levels (0.2, and 0.35 mm) at the selected target number of cycles. The variations of curvature range, moment range, and flexural rigidity as a function of number of cycles are given in Fig. 29. The rigidity of the measurements at two displacements started with 48 to 50 Nm^2 and demonstrated slight fluctuations during the cycling.

The curvature, moment, and flexural rigidity based on online monitoring data are presented in Fig. 30. The online monitoring showed a flexural rigidity of about 39 Nm^2, a little lower than that observed in measurements. This is mainly because different loading conditions were used in measurement and cycling. Overall, a steady response was exhibited over the whole cyclic testing period. Meanwhile, a negative curvature offset, -0.06 m^{-1}, was seen during the cyclic fatigue process.

Fig. 31 illustrates the failure position of the specimen. Fractographic study was conducted by using a stereo-optical microscope. The images of the lateral surface and fracture surfaces are presented in Fig. 32. Although some scratches are seen over the lateral surface, overall surface integrity was maintained to a certain extent. The fracture clearly occurred on the pellet-to-pellet interface. Mosaic cracks were developed in pellets. No apparent gap can be seen between pellet and cladding.

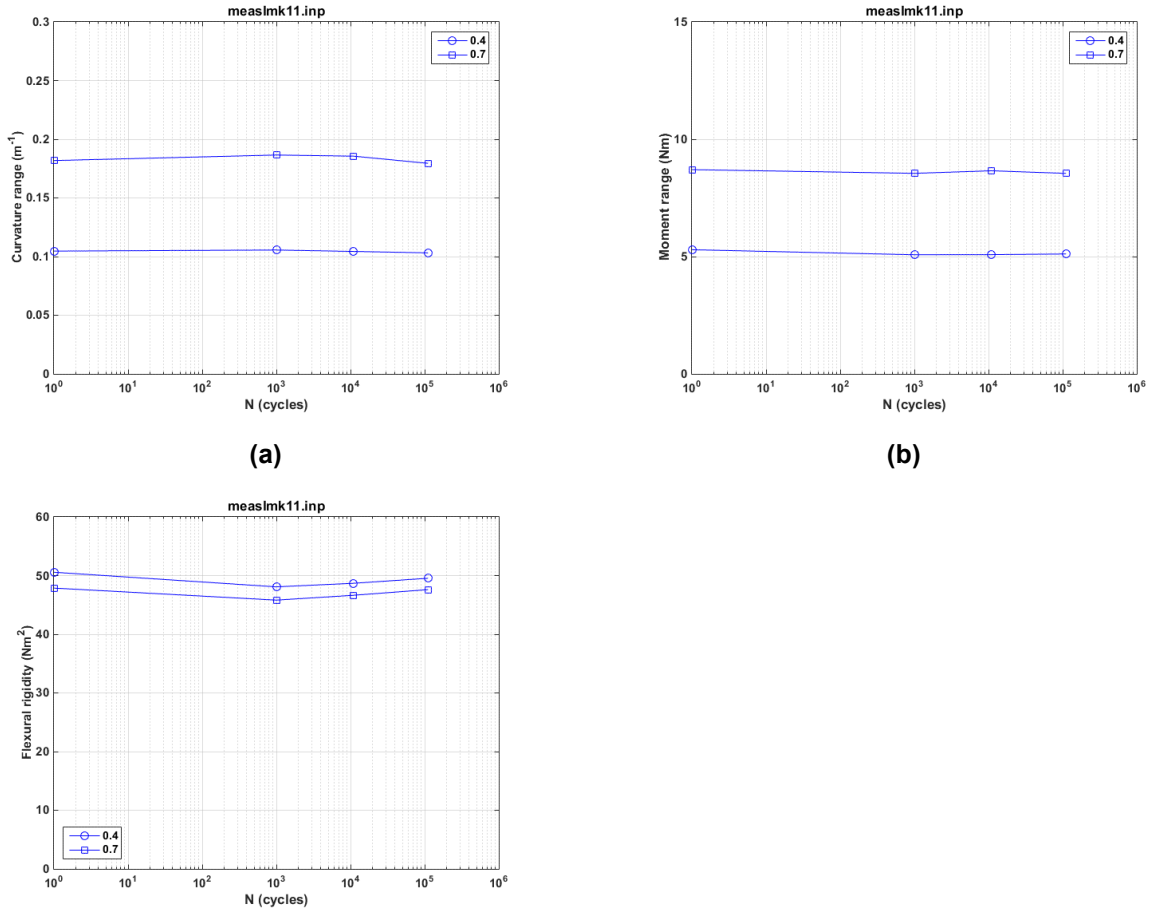

Fig. 29. Variations of (a) curvature range, (b) moment range, and (c) flexural rigidity as a function of number of cycles for LMK11/575B-D. Measurements were made with 0.2, and 0.35 mm relative displacements; $N_f = 3.55 \times 10^5$ cycles under ±8.64 N·m, 5 Hz.

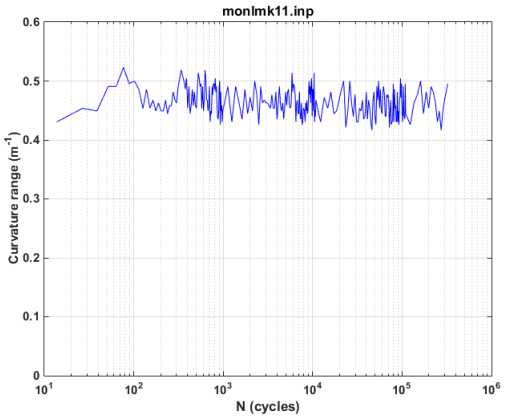

(a)

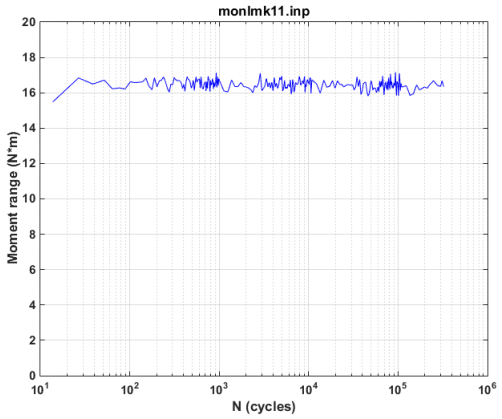

(b)

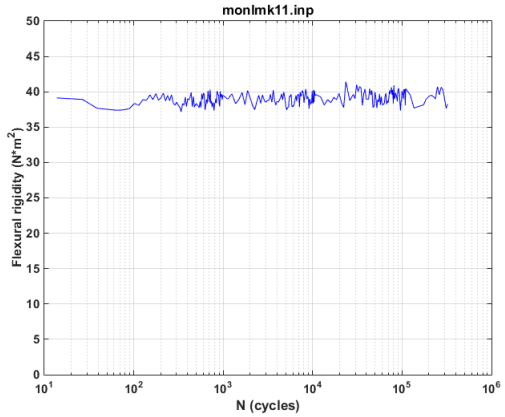

(c)

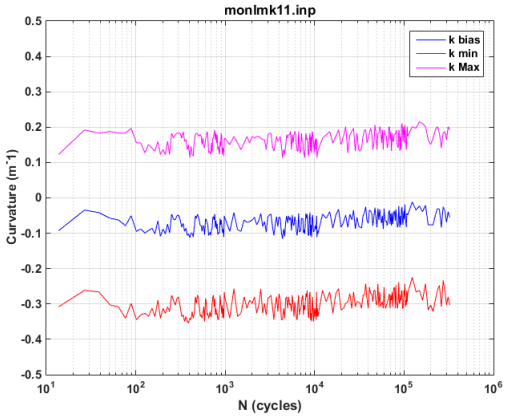

(d)

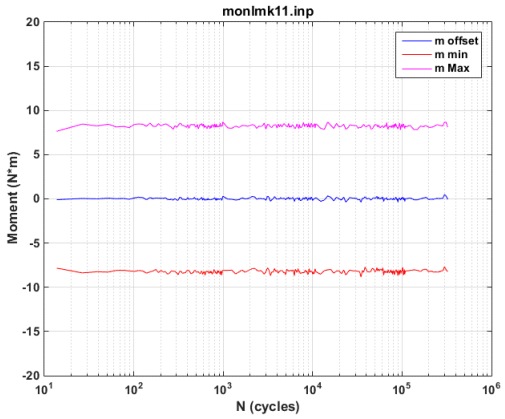

(e)

Fig. 30. Variations of (a) curvature range, (b) applied moment range, (c) flexural rigidity, (d) maximum and minimum values of curvature, and (e) maximum and minimum values of moment as a function of number of cycles for LMK11/575B-D; $N_f = 3.55 \times 10^5$ cycles under ±8.64 N·m, 5 Hz.

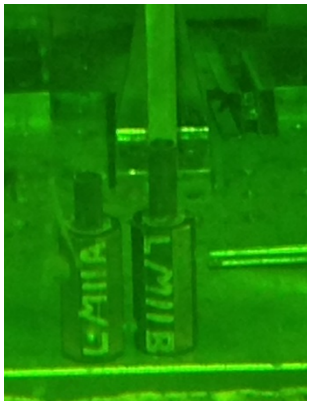

Fig. 31. Fracture segments for LMK11/574D-D; $N_f = 3.55 \times 10^5$ cycles under ±8.64 N·m, 5 Hz.

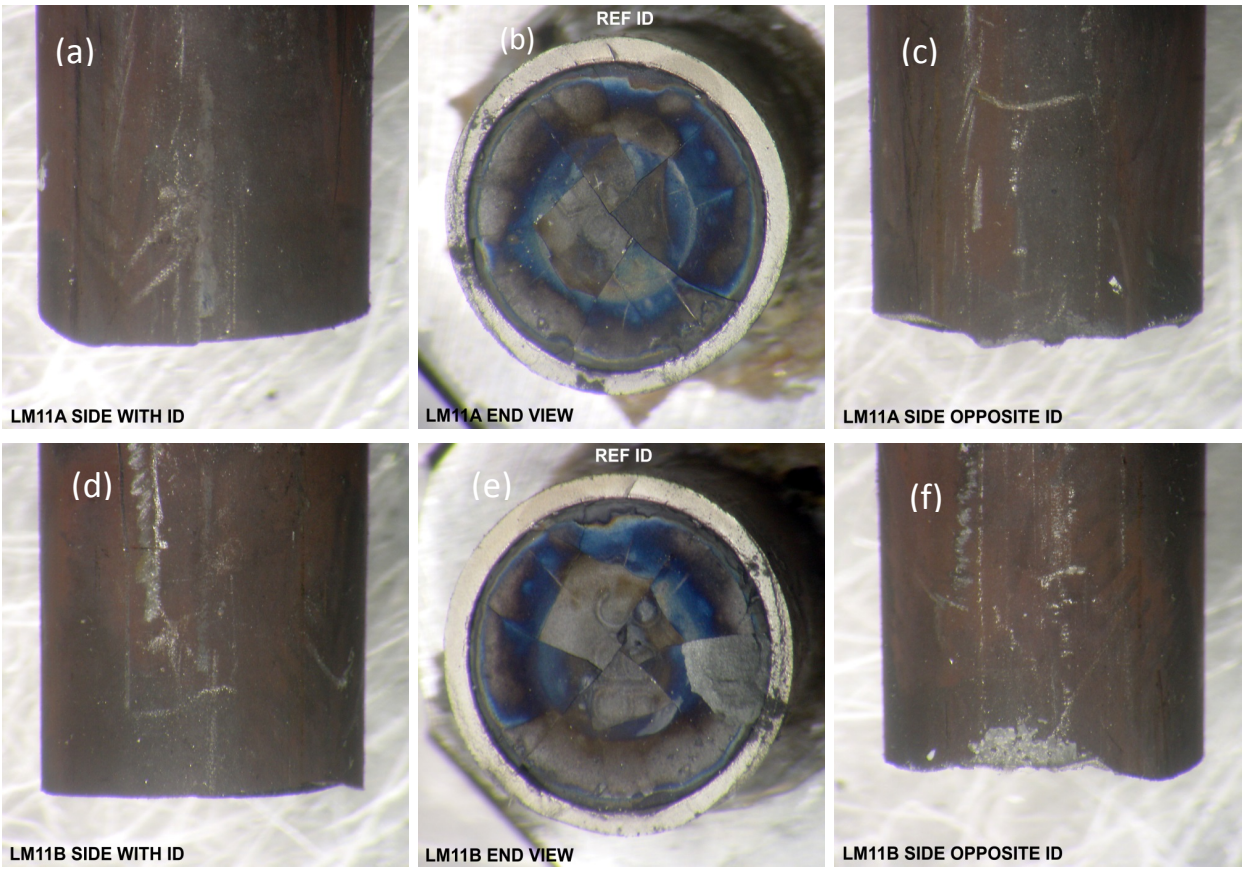

Fig. 32. Fracture segments for LMK11/575B-D. (a) and (d) show the specimen ID side of the segment on endcaps A and B; (b) and (e) show the mating fracture surface; and (c) and (f) show the opposite specimen ID side of segment on endcaps A and B.

5.10 LMK12/575B-A, ±7.11N·m, 5Hz

The test on the LMK12/575B-A rod was conducted under ±7.11 N·m, 5 Hz. The test stooped at the cycle number 7.58×10^6. The quasistatic measurements were conducted using two relative displacement levels (0.2, and 0.35 mm) at the selected number of cycles, and results are illustrated in Fig. 33. A small fluctuation occurred near 4 to 6×10^6 cycles. The reason for such fluctuation is not clear. However, the overall rigidity stayed around 30 to 38 Nm^2.

The curvature, moment, and flexural rigidity based on online monitoring data are presented in Fig. 36. The online monitoring showed a flexural rigidity variation of 24 to 29 Nm^2. At the same time, the curvature exhibited a little upward drift at the end of cycling of around 0.05 m^{-1}. Generally, the rigidity of this rod specimen is relatively lower compared to other LMK rods.

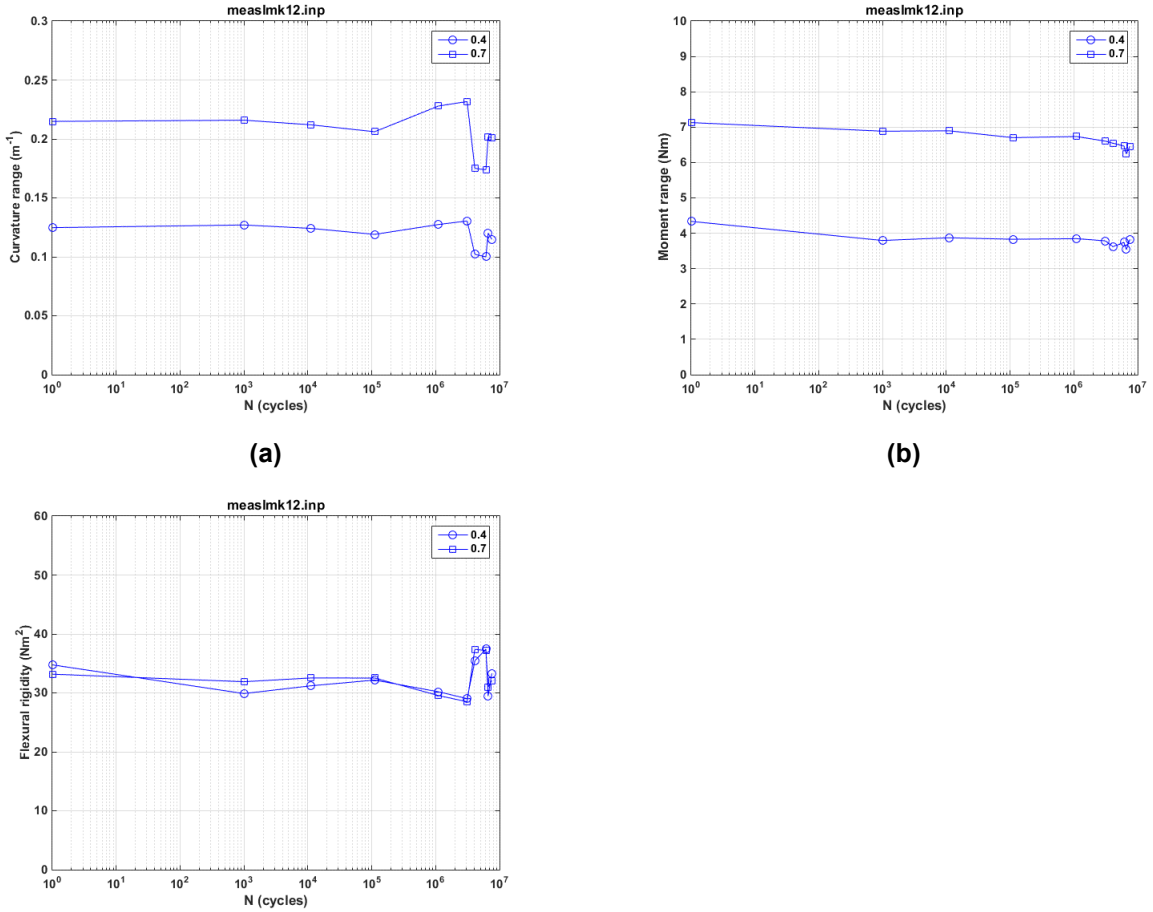

Fig. 33. Variations of (a) curvature range, (b) moment range, and (c) flexural rigidity as a function of number of cycles for LMK12/575B-A. Measurements were made with 0.2, and 0.35 mm relative displacements; N = 7.58×10^6 cycles under ±7.11 N·m, 5 Hz.

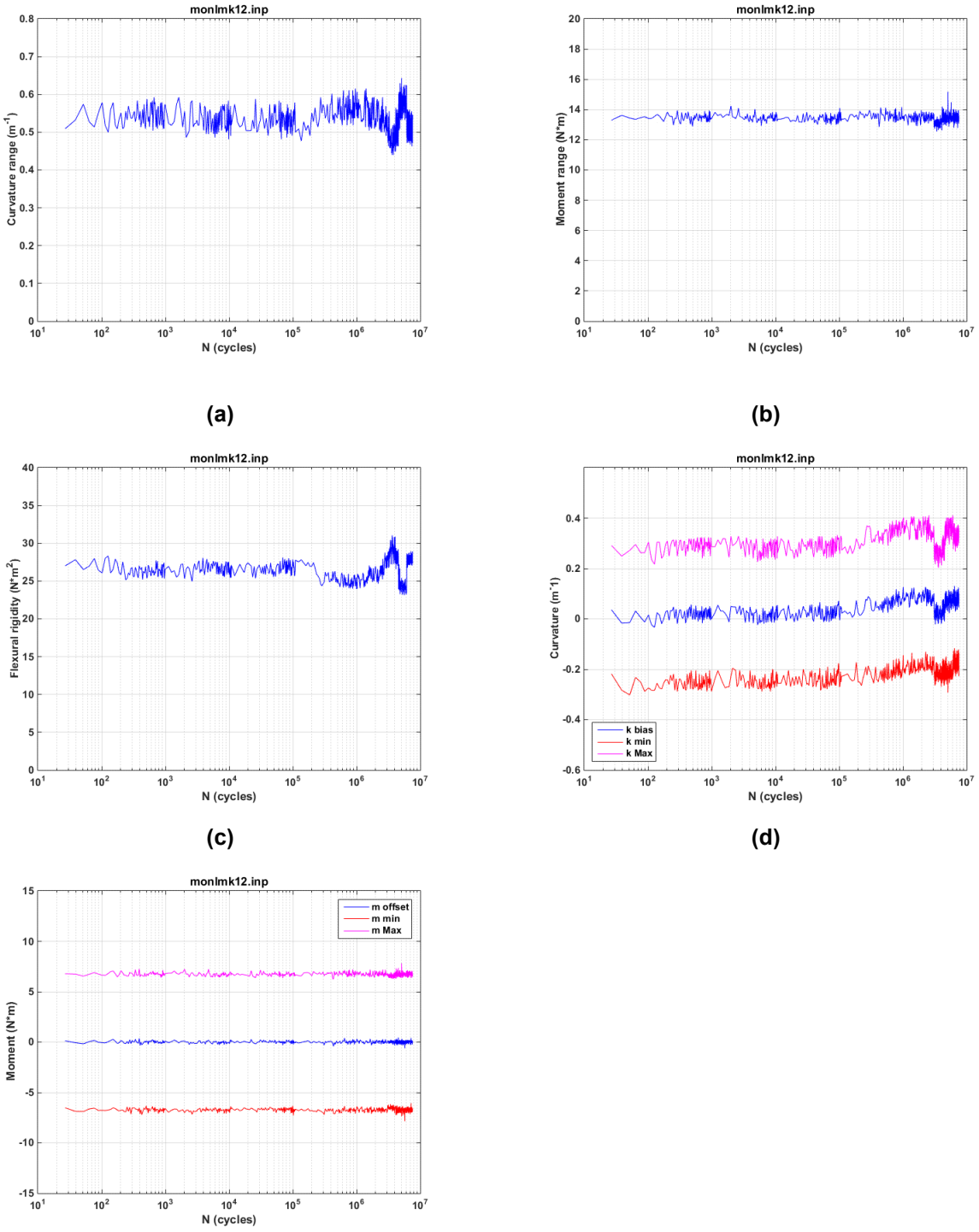

Fig. 34. Variations of (a) curvature range, (b) applied moment range, (c) flexural rigidity, (d) maximum and minimum values of curvature, and (e) maximum and minimum values of moment as a function of number of cycles for LMK12/575B-A; N = 7.58 × 10^6 cycles under ±7.11 N·m, 5 Hz.

6. DISCUSSIONS

Eleven SNF rod segments from the Limerick BWR were tested using the ORNL CIRFT, with one segment under static loading conditions and ten segments under dynamic loading conditions.

Under static unidirectional loading, a moment of 85 Nm was obtained at maximum curvature 4.0 m^{-1}. The specimen did not show any failure in three repeated loading cycles to nearly similar maximum curvature values.

Failure was observed when the SNF rod segments were cycled to various applied moments. The cycles to failure ranged from 1.22×10^5 to 4.70×10^6 when the amplitude varied from 15.2 to 7.6 N·m. The measurements at the interrupts indicated a range of flexural rigidity from 30 to 50 Nm^2. The online monitoring revealed that the flexural rigidity was a little lower due to the high level of loading, from 25 to 42 Nm^2. Generally, no substantial change of rigidity was observed based on online monitoring during the cyclic fatigue testing process.

The CIRFT dynamic testing results are summarized in Fig. 35 and Fig. 36. Overall, the decreasing trend of test specimen lifetime with the increasing amplitude is well defined.

The fatigue curves of the Limerick rods were compared with those of HB Robinson, North Anna, and Catawba (mixed oxide (MOX)) SNF in terms of amplitude of moment and strain, and results are given in Fig. 37, and Fig. 38.

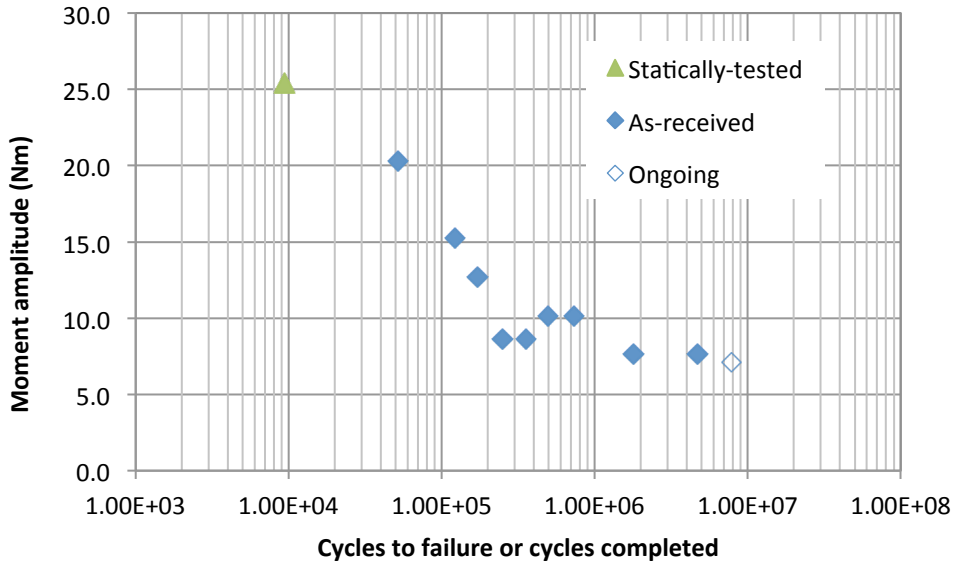

Fig. 35. Applied moment amplitude as a function of cycles to failure or cycles completed. The data point of pretested is based on a follow-up dynamic test of LMK01.

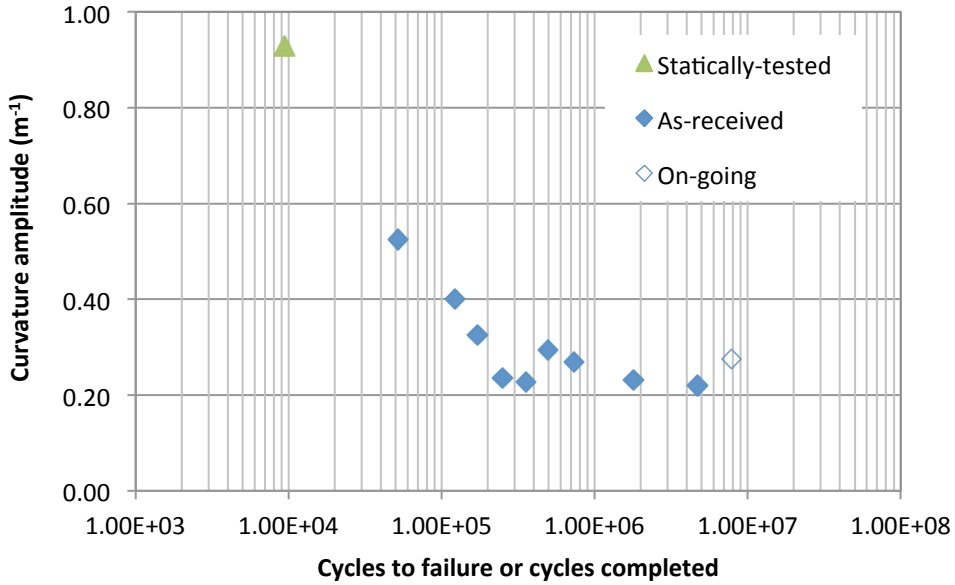

Fig. 36. Curvature amplitude as a function of cycles to failure or cycles completed. The data point of pretested is based on a follow-up dynamic test of LMK01.

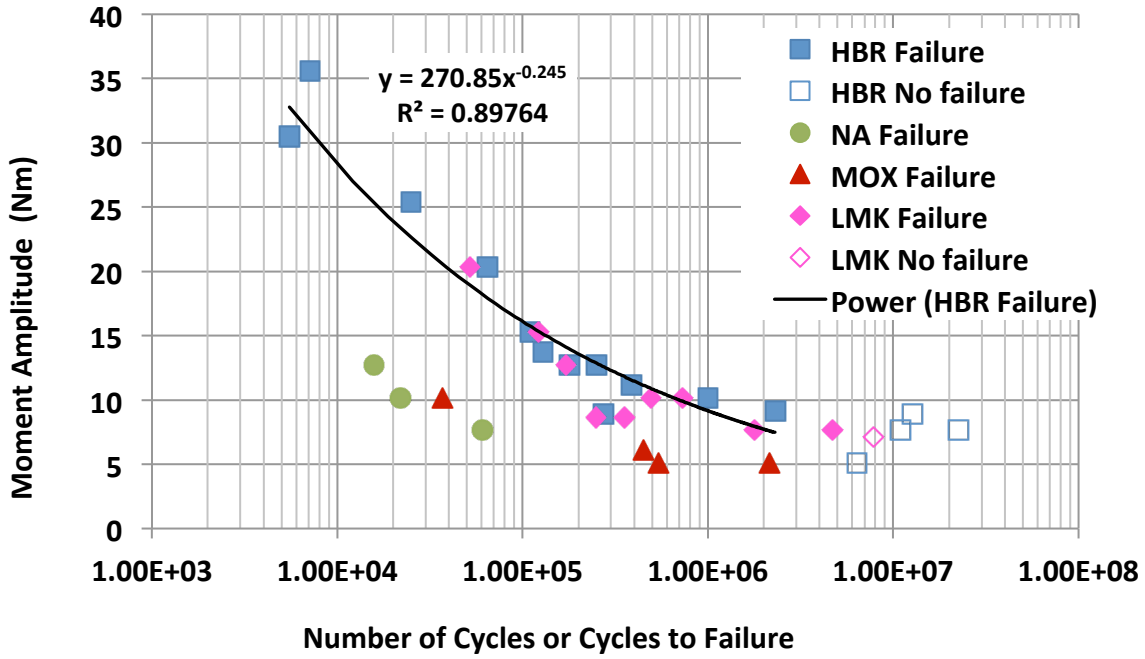

(a) All test points are presented.

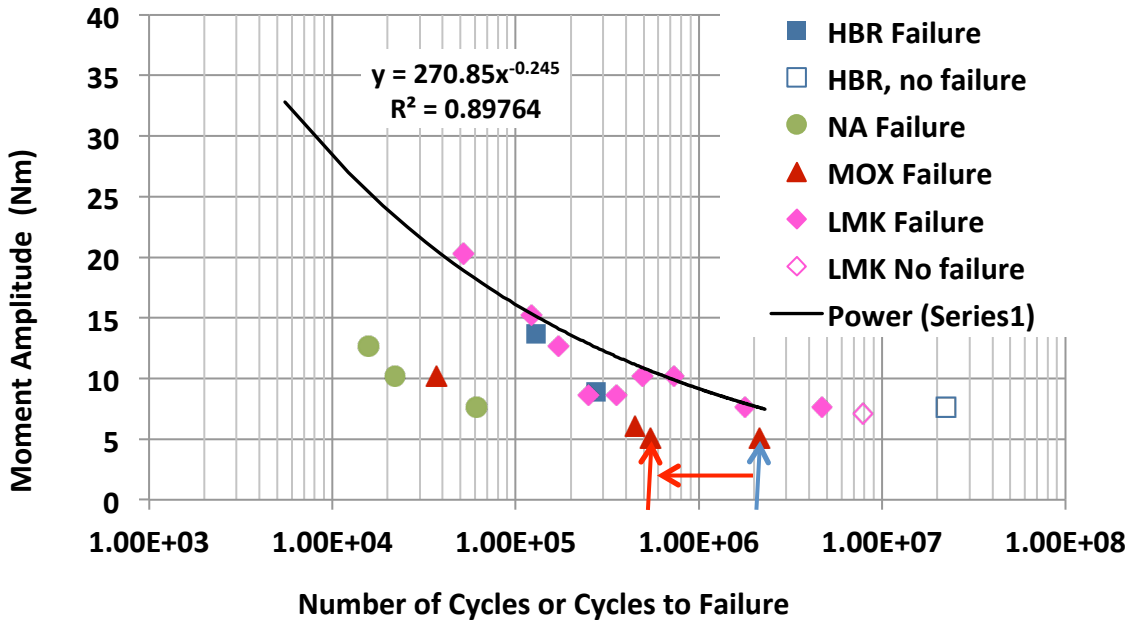

(b) HBR data points generated in NRC project are removed from the plot.

Fig. 37. Moment amplitudes as a function of number of cycles; results are based on CIRFT testing of various spent fuels at 5 Hz. The power function was obtained from curve fitting based on the HBR data set. The data point at the red arrow represents a test specimen with a two-foot drop, which shows significant reduction in fatigue life compared to data w/o drop (blue arrow).

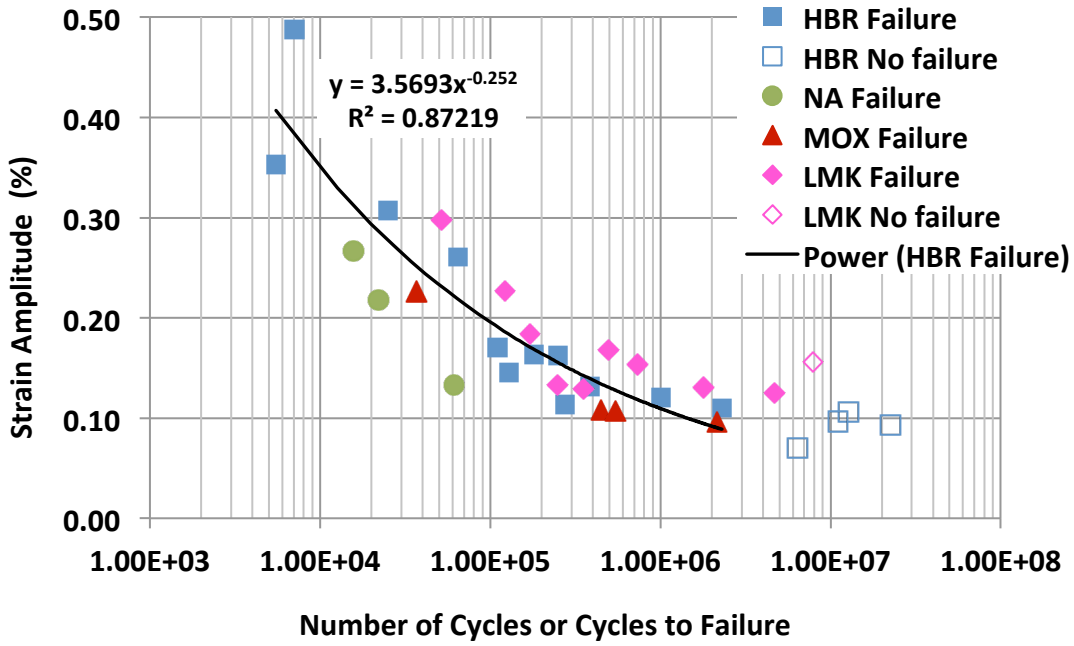

(a) All test points are presented.

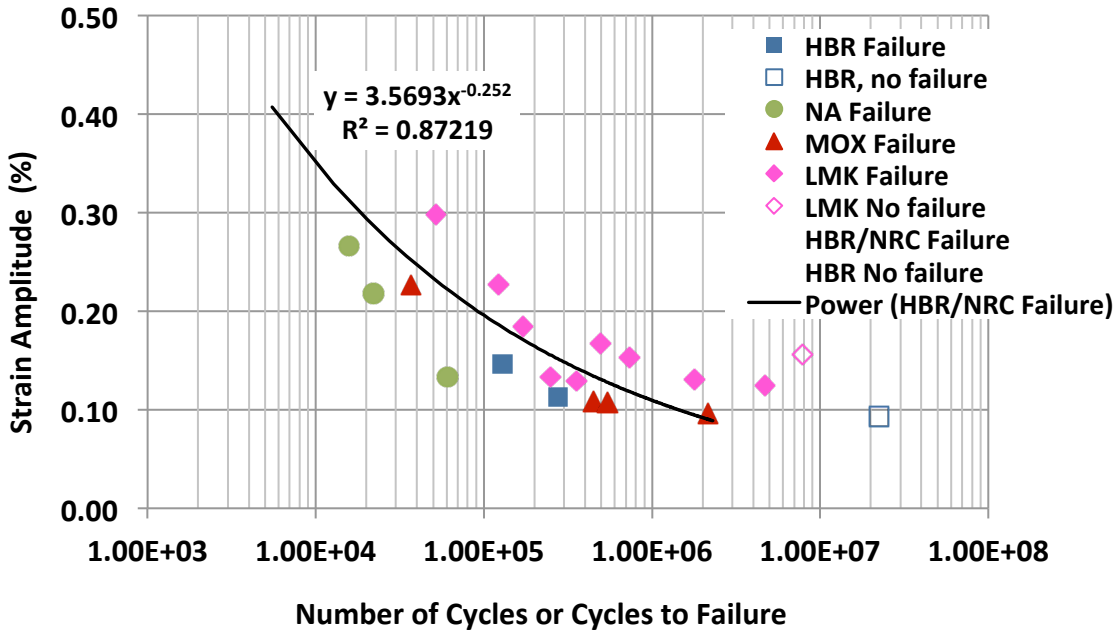

(b) HBR data points generated in NRC project are removed from the plot.

Fig. 38. Moment amplitudes as a function of number of cycles; results are based on CIRFT testing of various used fuels at 5 Hz. The power function was obtained from curve fitting based on the HBR data set.

ACKNOWLEDGMENTS

This research was sponsored by the DOE Used Fuel Disposition Campaign (UFDC) and NRC under DOE contract DE-AC05-00OR22725 with UT-Battelle, LLC. Authors thank ORNL program managers Bruce Bevard and Rob Howard for their support and guidance during the project; Chuck Baldwin for post-irradiation examination (PIE), Josh Schmidlin for fuel rod cutting and dimension measurement; Bryan Woody and Scot Thurman for hot-cell operation support; and Brian Sparks and Randy Parten for drawing and machining support.

REFERENCES

[1] J.-A. J. Wang, H. Wang, T. Cox, and Y. Yan, *Progress Letter Report on U-Frame Test Setup and Bending Fatigue Test for Vibration Integrity Study (Out-of-Cell Fatigue Testing Development–Task 2.3)*, ORNL/TM-2012/417, Oak Ridge National Laboratory, Oak Ridge, Tenn., August 2012.

[2] J.-A. J. Wang, H. Wang, and T. Tan, Reversal Bending Fatigue Testing, Pub. No. US 2013/0205911 A1, Aug. 15, 2013; also as US Patent No. US 8,863,585 B2, Oct. 21, 2014.

[3] H. Wang, J.-A. J. Wang, T. Tan, H. Jiang, T. S. Cox, R. L. Howard, B. B. Bevard, and M. E. Flanagan, "Development of U-frame Bending System for Studying the Vibration Integrity of Spent Nuclear Fuel," *Journal of Nuclear Materials,* **440**, 201–213 (2013).

[4] J.-A. J. Wang, H. Wang, T. Cox, and C. Baldwin, *Progress Letter Report on Bending Fatigue Test System Development for Spent Nuclear Fuel Vibration Integrity Study (Out-of-Cell Fatigue Testing Development–Task 2.4)*, ORNL/TM-2013/225, Oak Ridge National Laboratory, Oak Ridge, Tenn., July 2013.

[5] J.-A. J. Wang, H. Wang, B. B. Bevard, R. L. Howard, and M. E. Flanagan, *Reversible Bending Fatigue Test System for Investigating Vibration Integrity of Spent Nuclear Fuel During Transportation*, PATRAM 2013, DOE/NRC/DOT, San Francisco, Calif., August 18–23, 2013.

[6] J.-A. J. Wang and H. Wang, *The Development of Reversible Bending Fatigue Tester and Its Application to High Burn-up Spent Nuclear Fuel Integrity Study under Normal Transportation Vibration*, ORNL/TM-2013/573, August 2014. http://info.ornl.gov/sites/publications/Files/Pub47469.pdf

[7] J.-A. Wang and H. Wang, *2014 Semi-Annual Progress Letter Report on Used Nuclear Fuel Integrity Study in Transportation Environments*, prepared for US Department of Energy, ORNL/TM-2014/63, April 2014. http://info.ornl.gov/sites/publications/Files/Pub48652.pdf

[8] J.-A. J. Wang, H. Wang and H. Jiang, *FY14 Status Report: CIRFT Testing Results on High Burnup UNF*, ORNL/LTR-2014/310, September 2014. http://info.ornl.gov/sites/publications/Files/Pub51054.pdf

[9] J. E. Schmidlin, *Limerick fuel segmenting plan*, Oak Ridge National Laboratory, Nov. 3, 2014.

[10] C. A. Baldwin, *Fracture Surface Images of Selected CIRFT Tested Samples*, Oak Ridge National Laboratory, Feb. 27, 2015